2009-06

Transport Imaging developing an optical technique to characterize bulk semiconductor materials for next generation radiation detectors

Catalano, Sarah L.

Monterey, California: Naval Postgraduate School

NAVAL POSTGRADUATE SCHOOL

MONTEREY, CALIFORNIA

THESIS

TRANSPORT IMAGING:
DEVELOPING AN OPTICAL TECHNIQUE
TO CHARACTERIZE BULK SEMICONDUCTOR MATERIALS
FOR NEXT GENERATION RADIATION DETECTORS

by

Sarah L. Catalano

June 2009

Thesis Advisor:	Nancy M. Haegel
Second Reader:	Craig F. Smith

Approved for public release; distribution is unlimited

THIS PAGE INTENTIONALLY LEFT BLANK

REPORT DOCUMENTATION PAGE		Form Approved OMB No. 0704-0188

1. AGENCY USE ONLY *(Leave blank)*	2. REPORT DATE June 2009	3. REPORT TYPE AND DATES COVERED Master's Thesis

4. TITLE AND SUBTITLE Transport Imaging: Developing an Optical Technique to Characterize Bulk Semiconductor Materials for Next Generation Radiation Detectors	5. FUNDING NUMBERS
6. AUTHOR: Sarah L. Catalano	
7. PERFORMING ORGANIZATION NAME(S) AND ADDRESS(ES) Naval Postgraduate School Monterey, CA 93943-5000	8. PERFORMING ORGANIZATION REPORT NUMBER
9. SPONSORING /MONITORING AGENCY NAME(S) AND ADDRESS(ES) N/A	10. SPONSORING/MONITORING AGENCY REPORT NUMBER

11. SUPPLEMENTARY NOTES The views expressed in this thesis are those of the author and do not reflect the official policy or position of the Department of Defense or the U.S. Government.

12a. DISTRIBUTION / AVAILABILITY STATEMENT Approved for public release; distribution is unlimited	12b. DISTRIBUTION CODE

13. ABSTRACT (maximum 200 words)

Characterization of the mobility-lifetime product is critical to the development of new materials for semiconductor radiation detectors. An optical technique has been developed that allows for the direct determination of the minority carrier diffusion length, drift length, and mobility-lifetime product from a single image of the recombination luminescence in semiconductor materials. Excess carriers are generated using the electron beam in a scanning electron microscope. The charge is then drifted by applying an electric field, and the subsequent recombination luminescence is imaged by an optical microscope on a high-sensitivity CCD camera. The challenge in applying this technique to new materials for nuclear radiation detectors is the requirement for thick samples and the resultant need to characterize transport in three dimensions. In this work, initial research was performed on the simulations and analysis of experimental data required to characterize thick layers of high purity GaAs for nuclear radiation detectors. The first models were applied to extract values for surface recombination velocity, which plays a key role in determining the excess carrier distribution in bulk materials. Cathodoluminescence of one promising high Z material, $BiFeO_3$, is performed.

14. SUBJECT TERMS Cathodoluminescence, Diffusion, Drift, Mobility, Lifetime, Bismuth Ferrite, $BiFeO_3$, Semiconductor, Transport Imaging	15. NUMBER OF PAGES 79
	16. PRICE CODE

17. SECURITY CLASSIFICATION OF REPORT	18. SECURITY CLASSIFICATION OF THIS PAGE	19. SECURITY CLASSIFICATION OF ABSTRACT	20. LIMITATION OF ABSTRACT
Unclassified	Unclassified	Unclassified	UU

NSN 7540-01-280-5500

Standard Form 298 (Rev. 8-98)
Prescribed by ANSI Std. Z39.18

THIS PAGE INTENTIONALLY LEFT BLANK

Approved for public release; distribution is unlimited

TRANSPORT IMAGING: DEVELOPING AN OPTICAL TECHNIQUE TO CHARACTERIZE BULK SEMICONDUCTOR MATERIALS FOR NEXT GENERATION RADIATION DETECTORS

Sarah L. Catalano
ENS, United States Navy
B.S., United States Naval Academy, 2008

Submitted in partial fulfillment of the
requirements for the degree of

MASTER OF SCIENCE IN PHYSICS

from the

NAVAL POSTGRADUATE SCHOOL
June 2009

Author: Sarah L. Catalano

Approved by: Professor Nancy M. Haegel
Thesis Advisor

Professor Craig F. Smith
Second Reader

Professor James H. Luscombe
Chairman, Department of Physics

THIS PAGE INTENTIONALLY LEFT BLANK

ABSTRACT

Characterization of the mobility-lifetime product is critical to the development of new materials for semiconductor radiation detectors. An optical technique has been developed that allows for the direct determination of the minority carrier diffusion length, drift length, and mobility-lifetime product from a single image of the recombination luminescence in semiconductor materials. Excess carriers are generated using the electron beam in a scanning electron microscope. The charge is then drifted by applying an electric field, and the subsequent recombination luminescence is imaged by an optical microscope on a high-sensitivity CCD camera. The challenge in applying this technique to new materials for nuclear radiation detectors is the requirement for thick samples and the resultant need to characterize transport in three dimensions. In this work, initial research was performed on the simulations and analysis of experimental data required to characterize thick layers of high purity GaAs for nuclear radiation detectors. The first models were applied to extract values for surface recombination velocity, which plays a key role in determining the excess carrier distribution in bulk materials. Cathodoluminescence of one promising high Z material, $BiFeO_3$, is performed.

THIS PAGE INTENTIONALLY LEFT BLANK

TABLE OF CONTENTS

I. INTRODUCTION 1
A. SEARCHING FOR NUCLEAR WEAPONS, DIRTY BOMBS, AND SPECIAL NUCLEAR MATERIALS 1
B. NUCLEAR RADIATION DETECTORS 2
C. MILITARY RELEVANCE 3
D. THESIS OVERVIEW 4

II. IMPROVING HIGH RESOLUTION DETECTION IN ROOM TEMPERATURE SEMICONDUCTOR DEVICES 5
A. CURRENT SOLID STATE DETECTORS AND THEIR LIMITATIONS 5
B. NEW DETECTOR MATERIALS AND THEIR KEY PARAMETERS 6

III. TRANSPORT PARAMETERS 9
A. LUMINESCENCE IN SEMICONDUCTORS 9
B. DIFFUSION AND DRIFT 11
C. MOBILITY AND LIFETIME 12

IV. THEORETICAL APPROACH TO FIND MOBILITY-LIFETIME PRODUCT 15
A. TRANSPORT IMAGING 15
B. 2D ANALYSIS TO DETERMINE MOBILITY-LIFETIME PRODUCT 17
C. 3D ANALYSIS TO DETERMINE MOBILITY-LIFETIME PRODUCT 18

V. EXPERIMENTAL RESULTS OF MEASURING MOBILITY-LIFETIME PRODUCT IN GALLIUM ARSENIDE 21
A. 2D ANALYSIS OF MOBILITY-LIFETIME PRODUCT IN GALLIUM ARSENIDE 21
B. 3D ANALYSIS OF MOBILITY-LIFETIME PRODUCT IN GALLIUM ARSENIDE 34

VI. CATHODOLUMINESCENCE OF BISMUTH FERRITE 51

VII. CONCLUSIONS AND FUTURE RESEARCH 59

LIST OF REFERENCES 61

INITIAL DISTRIBUTION LIST 63

THIS PAGE INTENTIONALLY LEFT BLANK

LIST OF FIGURES

Figure 1. A Photon Excites an Electron from the Valence Band to the Conduction Band in a Direct Band Gap (a) and an Indirect Band Gap (b) 9
Figure 2. Types of Diffusion and Equations for Excess Minority Carrier Density 15
Figure 3. Excess Minority Carrier Distribution for 1D, 2D, and 3D Diffusion for L_{diff} =100 μm 16
Figure 4. Diffusion in 2D sample vs. 3D Sample 18
Figure 5. Distribution of Luminescence Generated in Spot Mode for InGaP (a), GaAs (b), and InGaAs (c) 22
Figure 6. JEOL 840A with Cathodoluminescence and Optical Microscope 23
Figure 7. SEM Stage 23
Figure 8. Micro CCD Camera 23
Figure 9. Optical Image of GaAs Sample with Contacts Fixed 1 mm Apart 24
Figure 10. Recombination Luminescence Images as a Function of Applied Field 27
Figure 11. Recombination Luminescence Images with Micro CCD Line for Data Extraction 28
Figure 12. Normalized Intensity Curves for Positive and Negative Applied E Fields 29
Figure 13. Linear Regression of Semi-Logarithmic Intensity Curves 31
Figure 14. Penetration Depth Charge Generation in GaAs as a Function of the Incident Electron Energy 35
Figure 15. Mathcad Simulation for L=50 μm Integrated with D=10, 20, 30, 40, and 50 μm 36
Figure 16. Mathcad Simulation for L=5 μm Integrated with D=10, 20, 30, 40, and 50 μm 37
Figure 17. Linear Regression to Approximate Slope When D=50 μm for a Range of Diffusion Lengths from 5 to 45 μm 38
Figure 18. Simulated Diffusion Length as a Function of Slope for Electric Fields from 0 to 90 V/mm 39
Figure 19. Schematic of Sample with Four Point Contact Geometry 41
Figure 20. IV Curve Measured at Inner and Outer Contacts on 4 Point Sample 42
Figure 21. Recombination Luminescence as a Function of Applied Current 46
Figure 22. Intensity as a Function of Distance for 4 Point Sample 47
Figure 23. Linear Regression to Determine Slope for Four Point Sample in the Absence of an Applied Field 48
Figure 24. CL of CYE-5 with 1 x 10^{-9} A Probe Current, 20 keV E Beam, and 2000X Magnification 52
Figure 25. CL of CYE-5 with 3 x 10^{-9} A Probe Current, 5 keV E Beam, and 5000X Magnification at 4.6 K 53

Figure 26. CL of Substrate with 3 x 10^{-9} A Probe Current , 20 keV E Beam, and 5000X Magnification 54
Figure 27. CL on BFO and $DyScO_3$ Substrate with 1x10^{-9} A Probe Current, 30 keV E Beam, and 2000X Magnification 56

LIST OF TABLES

Table 1. Values of Z for Semiconductors of Interest..... 8
Table 2. Band gap for Semiconductors of Interest. 10
Table 3. Slope, L_{diff}, L_{drift}, and $\mu\tau$ Product as a Function of Applied Electric Field..... 33
Table 4. L_{diff}, L_{drift}, and $\mu\tau$ Product for Each Applied Electric Field 40

THIS PAGE INTENTIONALLY LEFT BLANK

ACKNOWLEDGMENTS

I would like to thank Professor Nancy Haegel for her guidance and for creating a wonderful academic environment. The work in this paper is a result of her many suggestions and previous work.

I would like to thank Professor Eugene Haller and Professor R. Ramesh's lab group in the Department of Materials Science and Engineering at UC Berkley for providing BFO and GaAs samples.

This work was supported by the National Science Foundation and the Department of Homeland Security through the DNDO/NSF Academic Research Initiative (ARI) under Grant ECCS 0833007.

THIS PAGE INTENTIONALLY LEFT BLANK

I. INTRODUCTION

A. SEARCHING FOR NUCLEAR WEAPONS, DIRTY BOMBS, AND SPECIAL NUCLEAR MATERIALS

Following the attacks on September 11, 2001, President Bush cautioned that the "most horrifying" threat to the United States is a terrorist armed with nuclear capabilities [1]. In a press conference with Vladimir Putin, he stated, "Our highest priority is to keep terrorists from acquiring weapons of mass destruction [2]." The world's stockpile of nuclear materials, including highly enriched uranium, has proven to be vulnerable to mishandling and theft. As evidenced by the 2.7 million undocumented immigrants that have successfully passed Border Patrol and the Immigration and Naturalization Service, the United States borders are also highly susceptible to infiltration [3]. The combination of material availability and potential access poses a significant threat.

Before the attacks of September 11, the Secretary of Energy Advisory Board cautioned,

> The most urgent unmet security threat to the United States today is the danger that weapons of mass destruction or weapons usable material in Russia could be stolen and sold to terrorists or hostile nation states and used against American troops abroad or citizens at home. [4]

For at least 15 years, terrorist groups, including al Qaeda, have attempted to attain nuclear weapons or the knowledge and materials necessary to build a nuclear weapon. In Russia especially, nuclear reactors, weapons and highly enriched uranium are vulnerable to theft. In 2002, only 37% of the assailable nuclear material in Russia was protected, and only 17% of the highly enriched uranium stockpile in Russia had been destroyed [2].

There are limits on how much the United States can do to change the security standards of nuclear materials in other countries. This places a parallel

demand on the ability to detect incoming materials. At the same time, detecting a nuclear weapon when it is being smuggled into the United States is best described as searching for a needle in a haystack. In one year, 475 million people, 125 million vehicles, and 21.4 million import shipments arrive in the United States by land, air, and sea at 3,700 terminals and 301 ports of entry. Furthermore, there are nearly 100,000 miles of shoreline and 6,000 miles of borders with Canada and Mexico [3]. Finding a single nuclear weapon, dirty bomb, or special nuclear materials amidst this mass of people, traffic, and goods arriving in so many different locations is daunting.

Properly arming border patrol and law enforcement agencies with improved detectors can mitigate this problem. With research and development to modernize radiation detection technologies, over 800,000 state and local law enforcement officers can be better enabled and equipped to identify nuclear weapons or materials as they are smuggled into the country.

B. NUCLEAR RADIATION DETECTORS

Radiation detectors must do more than indicate that radiation is present. An effective detector must indicate the intensity of the radiation source and may also provide information to identify the type of radiation and its location. Particularly for national security purposes, distinguishing the type of radiation and measuring the energy spectrum are important. Specifically, Homeland Security and Border Patrol are interested in detecting gamma rays with energies that fall in the range of 10 keV to 10 MeV [5].

This may be achieved optimally with semiconductor materials in a detector paired with an appropriate electronic system that provides a signal output. This thesis focuses on the materials science of existing and potential semiconductors used for radiation detection. In semiconductor based radiation detectors, the energy from a single particle of radiation interacts with the semiconductor material resulting in a cascade of electron collisions. Consequently, free charge carriers, electrons and holes, are distributed in the material. With an applied

electric field, these carriers are transported out of the bulk material and recorded as an electronic pulse. The magnitude of the pulse is a function of the number of charge carriers that were initially created by the incident radiation. Therefore, the energy of the incident radiation is determined from the magnitude of the electronic pulse [5].

In order for this complicated process to occur, where a single quantum of radiation results in an electronic signal, the semiconductors used in detectors must meet stringent characteristics. For example, they must have quick and efficient transport of electrons and holes, or high mobility for the transport of free charge. They must also have a large number of protons in the nucleus, or be “high Z” materials. High Z materials have higher stopping power and, therefore, greater detection efficiencies. Ideally, they should also provide high resolution detection at room temperature. Finally, they must be based on materials that can be grown cost effectively in large volume. Chapter II discusses current radiation detectors and the need for next generation radiation detectors in detail.

C. MILITARY RELEVANCE

In April 2009, President Barack Obama announced, "The spread of nuclear weapons or the theft of nuclear material could lead to the extermination of any city on the planet [6]." A well-equipped terrorist organization could steal nuclear weapons or potentially build a crude bomb from stolen nuclear materials. After a terrorist group, like al Qaeda, attains a nuclear weapon, they could potentially attempt to detonate it in the United States. According to a 2003 report, a 10 kiloton bomb detonated in Grand Central Station in New York City on an average workday would kill half a million people and cause a trillion dollars in economic damage [2]. An attack of this magnitude would completely devastate the American way of life.

Detecting relevant threat materials in the vast amounts of imports and people that arrive daily in the United States is not an easy task for the 18,000 agencies responsible for national security. They must verify special nuclear

materials at ports of entry and monitor radiation on air, land, and sea borders between ports of entry. Equipping these agencies with improved radiation detectors is critical in the mission to prevent nuclear terrorism. National security demands the development of cost-effective nuclear detection capability to distinguish harmful radiation from non-threats.

D. THESIS OVERVIEW

This thesis seeks to explore the materials science required in an effort to improve radiation-detection by developing new high Z semiconductor radiation detector materials that can operate at room temperature. Current detectors and their limitations are discussed. In addition to current detectors, the design requirements for next generation radiation detectors are reviewed. Important materials science parameters are introduced, as they are crucial in understanding the tools required for analyzing potential materials used in future detectors. The mobility-lifetime ($\mu\tau$) product is a critical parameter for any material used in radiation detection. A new method for characterizing this parameter using optical imaging in a scanning electron microscope is developed. This technique is then illustrated experimentally on gallium arsenide. Bismuth ferrite (BFO) is a new promising high Z material that is simultaneously ferroelectric and magnetic. Cathodoluminescence of BFO is performed as it has potential to be used in next generation radiation detectors. Finally, conclusions and suggestions for future research are presented.

II. IMPROVING HIGH RESOLUTION DETECTION IN ROOM TEMPERATURE SEMICONDUCTOR DEVICES

A. CURRENT SOLID STATE DETECTORS AND THEIR LIMITATIONS

Silicon and germanium were the initial semiconductors used in solid state radiation detectors. They are unique materials because they can be grown in bulk with relatively high purities. For any semiconductor-based radiation detector, the challenge is to develop a method to optimize signal collection over a volume of ample size to completely stop the incident radiation. Since silicon (Z=14) is a lower Z material than germanium (Z=32), this task is more difficult in silicon. In both cases, however, thick high purity materials can be grown to create fully depleted p-i-n diodes for their charge collection.

The materials in current use have significant disadvantages. Lithium drifted silicon and germanium need to be cryogenically cooled at all times to support large depleted regions in the reverse bias configuration [5]. Even high purity germanium must be cooled with liquid nitrogen. Cooling these materials increases the size and cost of these detectors considerably and makes them unrealistic choices for most national security applications.

Operationally, the detectors must distinguish between radiation from the target nuclear material and that from other mundane sources. Common products like kitty litter and ceramics contain naturally occurring radioactive materials. With over 32,000 sea-going containers, 2 million people, 1.8 millions pieces of luggage, and over 200,000 general aviation flights entering the country daily, the economy cannot afford the delays caused by detectors that cannot differentiate between radiation sources. Constricting the flow of imports with intensified inspections on borders raises transaction costs and makes the United States' ports less competitive for overseas business. For example, five inspectors take approximately three hours to thoroughly inspect a loaded 40-foot container. However, in the two ports that receive some of the highest traffic in

the country, the ports of Long Beach and Detroit, customs officials must clear one container in every 20 seconds and one truck every 12 seconds, respectively [3]. With this large quantity of shipping, a detector that can distinguish naturally occurring radiation in kitty litter and ceramics from weapons of mass destruction is paramount.

A detector's energy resolution is its ability to identify the nuclear isotopes that are producing the radiation. A semiconductor with high-energy resolution can distinguish harmful radiation sources from innocuous ones. The community uses the energy resolution for the gamma ray of ^{137}Cs at 662 keV as a benchmark to compare semiconductors. In order to achieve high resolution, a radiation detection material must provide the maximum average number of charge carries while minimizing random variance between events [5].

Cadmium zinc telluride (CZT) is frequently used in current detectors and is arguably the most successful emerging semiconductor material for room temperature detectors. Cadmium and tellurium are high Z and therefore, CZT has a very high atomic weight. Though CZT has high Z and can operate at room temperature, this semiconductor has specific material challenges. The material cannot achieve high resolution compared to germanium for the gamma-ray spectrum. CZT has relatively poor hole transport and has shown poor energy resolution of less than 1% for the benchmark 662 keV gamma ray for detectors about 1 cm^3 in size. In comparison, germanium exhibits an energy resolution of .15%.

B. NEW DETECTOR MATERIALS AND THEIR KEY PARAMETERS

To meet national security needs, a low cost, high z room temperature detector that can distinguish between types of radiation must be built. Materials science plays a crucial role in developing a new detector that satisfies the operational requirements. Many material parameters must be analyzed to determine if a new semiconductor could be utilized in an effective detector.

The band gap is a key parameter in characterizing semiconductors. A large band gap requires a relatively large amount of energy to create electron hole pairs. These electron hole pairs are the crucial information carriers that allow a quantum of radiation incident on a semiconductor to generate an electronic signal. However, a small band gap allows for thermal excitation that leads to dark currents and high conductivity that obscure the output signal. Therefore, the semiconductors being investigated generally have band gaps between 0.7 and 3 eV [5].

The semiconductor must be able to handle the occurrence of a high rate of nuclear radiation interactions. This is important when there is strong radioactive background noise or when the radiation source is particularly strong. Background gamma ray flux is usually greater than 10^3 $m^{-2}s^{-1}$ and energy resolution requires that distinct events hardly ever coincide [5]. Therefore, materials used in radiation detectors must sustain fast readout of the electron-hole pairs in the energy cascade. In other words, a semiconductor must have high mobility, ideally for both types of charge carriers, to be effective in radiation detection.

The semiconductor's efficiency at detecting nuclear radiation is crucial. Although detector efficiency is a dynamic and complicated criterion, it depends largely on the atomic number of the material. The atomic number is often referred to as Z or the atomic weight of the material. Table 1 shows the Z of semiconductors of interest.

Si	Z=14
Ge	Z=32
GaAs	Z=31, 33
CdZnTe	Z=48, 30, 52
$BiFeO_3$	Z=83, 26, 24

Table 1. Values of Z for Semiconductors of Interest.

As Z increases, detector efficiency increases. High Z materials have been the focus of research and development teams working to build the next generation gamma ray detector. One of the largest limitations on selecting a semiconductor is the size to which material can be grown without impurities and defects. If a material has higher density and higher Z, a thinner sample could effectively stop the same amount of radiation as a thicker sample with lower density and lower Z. A high Z material has greater stopping power for incident radiation and may potentially mitigate the issues that arise from growing high purity, defect-free crystals in large quantities.

III. TRANSPORT PARAMETERS

A. LUMINESCENCE IN SEMICONDUCTORS

In semiconductors, luminescence arises from the interaction of electrons between the valence band, the highest energy filled band, and the conduction band, which is above the valence band and is empty at T=0 K [7]. The band gap (E_g) is the energy difference between these two bands. If the bottom of the conduction band is directly above the top of the valence band in momentum space, the material is said to have a direct band gap. Conversely, if the valence band maximum and the conduction band minimum are not aligned in momentum space, the material is said to have an indirect band gap. Figure 1 illustrates both direct (a) and indirect (b) band gaps [8]. The y-axis is energy. The x-axis is the wave vector k and is related to momentum as $p = \frac{hk}{2\pi}$ where h is Planck's constant.

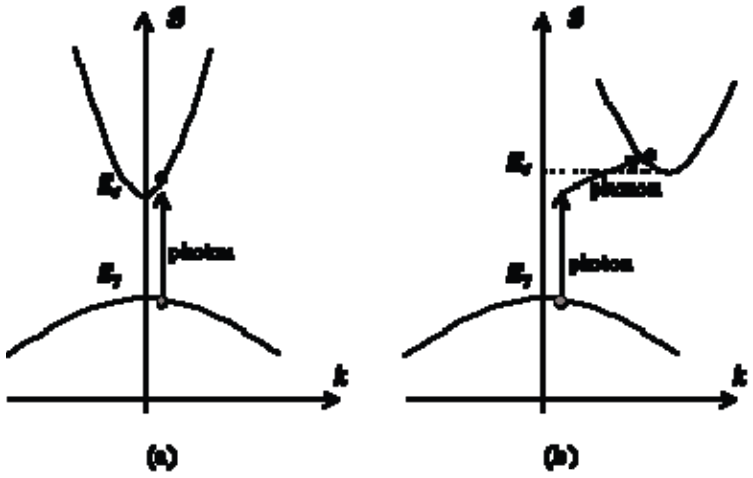

Figure 1. A Photon Excites an Electron from the Valence Band to the Conduction Band in a Direct Band Gap (a) and an Indirect Band Gap (b)

The band gap in most semiconductors is typically on the order of 1-3 eV. Table 2 gives the band gap of several important semiconductors.

Material	Band gap (eV)	Type of band gap
Ge	0.67	Indirect
Si	1.11	Indirect
GaAs	1.43	Direct
CdTe	1.56	Direct
$BiFeO_3$	~2.7	Direct

Table 2. Band gap for Semiconductors of Interest.

Assume light with photon energy $h\nu$ is incident on a material with band gap E_g. If the photon energy is greater than the band gap (or $h\nu > E_g$), the photon has sufficient energy to excite an electron out of the valence band and into the conduction band. The result is an extra electron in the conduction band and a hole in the valence band. This results in an electron-hole pair. These electrons and holes can move within the bands freely and contribute to the conductivity of the material. An electron in the conduction band may recombine with a hole in the valence band and emit a photon. The photon emitted has approximately the same energy as the material's band gap such that:

$$\Delta E = \frac{1.24}{\lambda}$$

where E is the energy in eV and the wavelength (λ) is measured in microns.

Luminescence is the excitation of a material that induces this emission of light as described above. Many sources of excitation can be used to produce luminescence in a material. Photoluminescence (PL) is the process of exciting the material with an incident photon beam (e.g., a laser) while cathodoluminescence (CL) utilizes an electron beam to generate photon

emission. Processes like CL and PL result in a non-equilibrium concentration of electron-hole pairs and resulting recombination that may be analyzed to reveal important material parameters such as free carrier diffusion and drift.

B. DIFFUSION AND DRIFT

When there is an external excitation source, additional carriers are created. Electron and hole concentrations per volume prior to excitation are denoted n_{no} and p_{no} respectively. Furthermore, electron and hole concentrations per volume after excitation are denoted n_n and p_n respectively. If the sample is n type, the majority carriers are electrons and the minority carriers are holes. If the sample is p type, the majority carriers are holes and the minority carriers are electrons [9]. In semiconductor materials, minority and majority carriers can have different diffusion and drift rates.

Diffusion occurs in a semiconductor when there is a carrier concentration gradient produced by some excitation. Materials have a tendency to spread the charge population uniformly across the material's volume and, therefore, the carriers migrate or diffuse from a region of high concentration to low concentration. The diffusion coefficient (D) quantifies the diffusivity of a material. The diffusion coefficient is found using the Einstein relation

$$D = \frac{kT\mu}{e}$$

where k is Boltzmann's constant, T is the temperature, e is the charge of an electron, and μ is the mobility. Mobility is a parameter that measures the ease with which electrons and electron holes are able to move in a material. As mobility differs for electrons and holes due to their respective effective masses, the diffusion coefficient also differs for electrons and holes.

The diffusion length (L_{diff}) is the average distance a carrier will travel before recombining and is calculated by

$$L_{diff} = \sqrt{D\tau} = \sqrt{\frac{\mu\tau kT}{e}}$$

where D is the diffusion coefficient and τ is the excess carrier lifetime.

Drift is the net motion of carriers in a material due to an applied bias and consequently drift length (L_{drift}) measures the average distance a carrier will travel due to an applied electric field and is defined as

$$L_{drift} = \mu\tau E$$

where E is the applied electric field. Although an applied E field drives the drift and a concentration gradient drives diffusion, note that $\mu\tau$ appears explicitly in both of the equations for L_{drift} and L_{diff}. The mobility-lifetime product (or $\mu\tau$ product) is a crucial parameter affecting the charge collection in semiconductor materials for nuclear radiation detection.

C. MOBILITY AND LIFETIME

In the absence of an electric field, electrons and holes move randomly within a semiconductor and, consequently, the net movement does not appear to occur in any particular direction. However, electrons are accelerated in an applied electric field. The drift velocity (v_{drift}) measures the electrons and holes' movements due to the applied field. The constant of proportionality that relates the drift velocity to the applied electric field is mobility (μ):

$$v_{drift} = \mu E$$

where E is the electric field or in terms of the effective mass of the drifting particle:

$$\mu = \frac{e\tau}{m^*}$$

where m* is the effective mass, τ is the lifetime or scattering time, and e is the charge of an electron. Since the effective masses of electrons and holes are

different, the mobility also differs for electrons and holes. The lifetime is the amount of time a particle can move before encountering and interacting with another particle. For example, in CL, after the sample is bombarded with an electron beam, the excess charges begin to diffuse due to the carrier concentration gradient and stop when they recombine with an electron or hole. The average time that elapsed before the electron recombines with holes, or vice versa, is the minority carrier lifetime.

In a doped semiconductor, the lifetime for minority carriers (e.g., holes in n type material) is inversely proportional to the population of majority carriers (e.g., electrons in n type material). In this case, the lifetime, τ, is given by

$$\tau = \frac{B}{n}$$

where B is a recombination coefficient and n is the majority carrier concentration. This means that the lifetime of minority carriers is a constant, depending on majority doping, if the majority carrier population is held constant.

THIS PAGE INTENTIONALLY LEFT BLANK

IV. THEORETICAL APPROACH TO FIND MOBILITY-LIFETIME PRODUCT

A. TRANSPORT IMAGING

The overarching goal of the transport imaging approach described in this work is to directly determine a value for L_{diff} and, consequently, obtain the $\mu\tau$ product of a material from a single optical image. This can be achieved by evaluating the carrier distribution and resulting luminescence in a sample. The process begins with an external excitation, such as the incident electron beam in an SEM, which creates a concentration gradient. The resulting distribution of the excess minority carriers depends on the thickness of the sample and the diffusion length. If the sample is confined in two dimensions like a nanowire, diffusion occurs only in one dimension (1D). If the sample is a thin layer (100-1000 nm), the carriers diffuse two dimensionally (2D). If the sample is thick (≥1 μm), the diffusion occurs in three dimensions (3D). Figure 2 illustrates the three different types of diffusion and shows how the excess minority carrier density decreases in each case along a given direction:

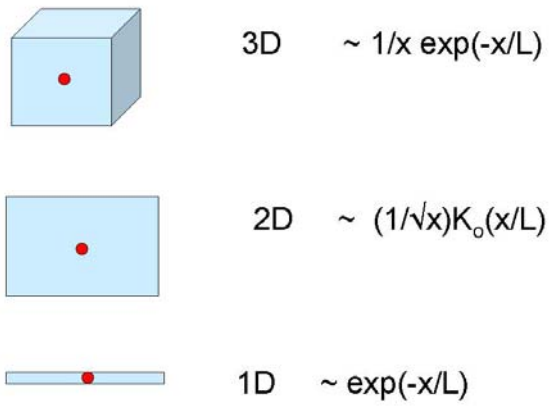

Figure 2. Types of Diffusion and Equations for Excess Minority Carrier Density

In the 2D case, diffusion takes place in accordance with K_o, a zeroth-order modified Bessel function of the second kind. All of these expressions assume that recombination at the surface is negligible and can be neglected. The excess minority carrier density drops off much more rapidly in the 3D case then in the 1D or 2D case due to the $\frac{1}{|x|}$ term in the 3D case. The 1D case is trivial as the density simply decreases as a decaying exponential as x moves further from the source and L_{diff} can be easily extracted. The 2D and 3D cases require more detailed analysis. Figure 3 illustrates the excess minority carrier distribution as a function of distance from the generation point for 1D, 2D, and 3D samples for L_{diff} =100 μm.

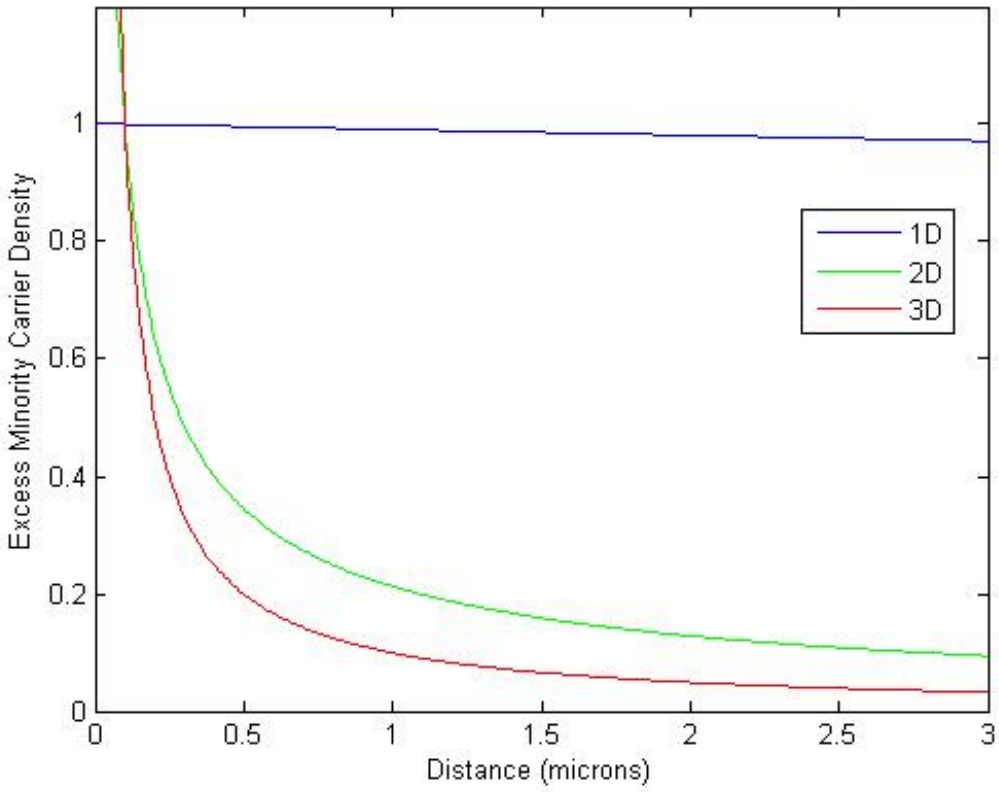

Figure 3. Excess Minority Carrier Distribution for 1D, 2D, and 3D Diffusion for L_{diff} =100 μm

B. 2D ANALYSIS TO DETERMINE MOBILITY-LIFETIME PRODUCT

In the 2D case, where the sample is a thin layer and diffusion is confined to a plane, the excess minority carrier density decreases like a zeroth-order modified Bessel function of the second kind. An incident beam generates excess carriers. The charges drift in an applied electric field. Recombination luminescence is imaged on a high- sensitivity camera. The intensity is extracted from the recombination luminescence images.

Mathematically, in the limit of large x, the Bessel function K_p (x) can be approximated by a decaying exponential of the form [10]:

$$K_p(x) \approx e^{-x} + O\left(\frac{e^{-x}}{x}\right)$$

where $O\left(\frac{e^{-x}}{x}\right)$ represents the error associated with this approximation. Therefore, the error is less than a constant times x^n. At a distance from the point of excitation significantly greater than the material's diffusion length, the Bessel function that models the distribution can be approximated by a decaying exponential function as shown [11]:

$$` I = K_o\left(\frac{|x|}{L_{diff}}\right) \square e^{Cx}$$

where I is the excess minority carrier density and

$$C = \frac{L_{drift}}{2L_{diff}^2} + \frac{-\sqrt{L_{drift}^2 + 4L_{diff}^2}}{2L_{diff}^2} = \frac{L_{drift} - \sqrt{L_{drift}^2 + 4L_{diff}^2}}{2L_{diff}^2}$$

$$= \left(\frac{e}{2kT}\right)E - \sqrt{\left(\frac{e}{2kT}\right)^2 E^2 + \frac{1}{L_{diff}^2}}$$

Consequently, if the applied electric field is accurately known, the diffusion length of the material can be derived from the slope of the natural log of intensity plotted against distance. As $L_{diff} = \sqrt{\frac{\mu\tau kT}{e}}$, the $\mu\tau$ product can be directly determined.

C. 3D ANALYSIS TO DETERMINE MOBILITY-LIFETIME PRODUCT

In the 3D case, an incident beam generates excess carriers and applying an electric field drifts the charges. However, when an electric field is applied, the charges may drift in the plane of the field but will also diffuse in the z direction of the material due to the existing concentration gradient. Figure 4 is an illustration of the difference between 3D and 2D excess minority carrier distribution.

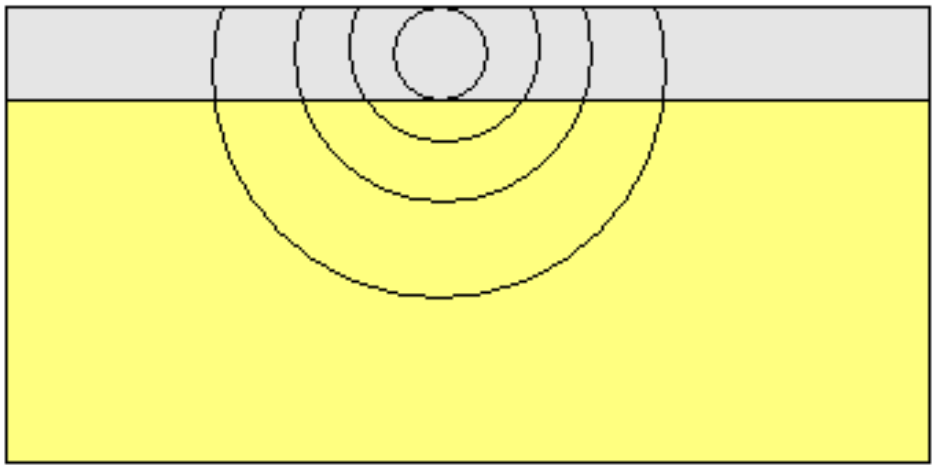

Figure 4. Diffusion in 2D sample vs. 3D Sample

Since recombination does not occur exclusively at the material's surface, the luminescence must be integrated in the z direction. The intensity along the x axis can be modeled as:

$$I = \int_0^D \left(\frac{g}{4 \cdot Ldiff^2 \cdot \pi} \right) \cdot \left(e^{\frac{S \cdot x}{2 \cdot Ldiff^2}} \right) \cdot \left(\frac{e^{\frac{-\sqrt{S^2 + 4Ldiff^2}}{2L_{diff}^2} \cdot \sqrt{x^2+y^2+z^2}}}{\sqrt{x^2+y^2+z^2}} \right) dz$$

where g is the generation rate of the incident electron beam and D is the depth of the material. The $\left(\frac{g}{4 \cdot L_{diff}{}^2 \cdot \pi}\right)$ term is a constant based on the electron beam being used. The $\left(e^{\frac{S \cdot x}{2 \cdot L_{diff}{}^2}}\right)$ term models the effect of an applied electric field. The $\sqrt{x^2 + y^2 + z^2}$ term reflects the 3D diffusion. This model assumes that diffusion is occurring in 3D and drift is occurring only in 1D. Integrating through each layer is necessary in the 3D case to find the total excess minority carrier charge distribution throughout the material's thickness.

Using the model, a numerical correlation can be found relating the slope of the semi-logarithmic plot of the integrated intensity versus distance to the diffusion length. The experimental slope then yields a diffusion length through this correlation. After finding the diffusion length, the $\mu\tau$ product is calculated.

THIS PAGE INTENTIONALLY LEFT BLANK

V. EXPERIMENTAL RESULTS OF MEASURING MOBILITY-LIFETIME PRODUCT IN GALLIUM ARSENIDE

A. 2D ANALYSIS OF MOBILITY-LIFETIME PRODUCT IN GALLIUM ARSENIDE

Using the optical image of the recombination luminescence in a material, a technique has been developed that provides an avenue to directly determine the minority carrier diffusion length, drift length, and, consequently, the $\mu\tau$ product. This technique utilizes the excess charge generation capabilities of a scanning electron microscope (SEM) in coordination with an optical microscope on a high sensitivity CCD camera. The electron beam from the SEM is incident on the sample and generates excess carriers. These excess carriers are then drifted with an applied electric field. Next, the recombination luminescence from the charge distribution is imaged using the optical microscope on a high sensitivity camera.

This approach is unique from standard CL because spatial resolution of the light emission is preserved. In CL the beam is typically scanned across the sample and the data regarding the location of the source of luminescence is lost. However, in transport imaging, the electron beam is not scanned and recombination luminescence is collected from its point of origin. Therefore, the spatial information is retained.

The SEM is a JEOL 840A model that can be used in spot mode, line mode, and picture mode to generate the charges. These modes represent the regions over which the SEM generates charge. Spot mode is the most relevant to this thesis and Figure 5 gives an example of the distribution of luminescence generated in spot mode for InGaP (a), GaAs (b), and InGaAs (c):

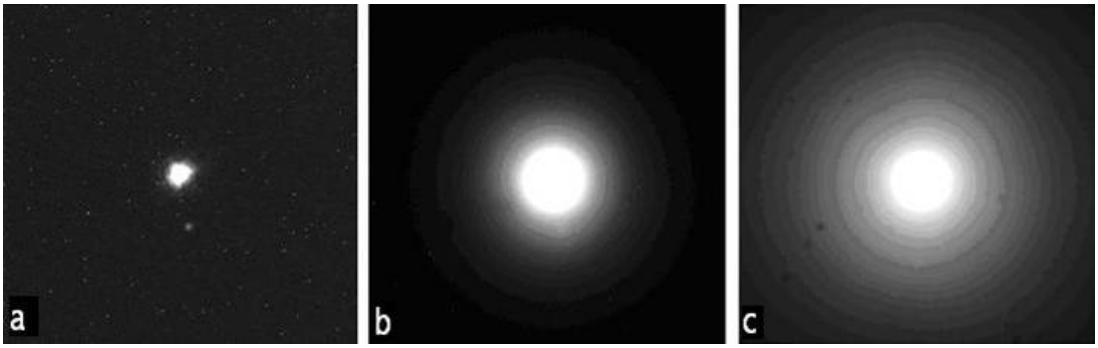

Figure 5. Distribution of Luminescence Generated in Spot Mode for InGaP (a), GaAs (b), and InGaAs (c)

An optical microscope is fed into the main chamber of the vacuum-sealed SEM. This optical microscope is connected to a 1284 X 1472 pixel CCD array [12]. The magnification of the optical system is about 20X and the resolution of the system is 0.4 $\frac{\mu m}{pixel}$. In an effort to minimize the thermal noise in the detector, the Apogee CCD camera is thermoelectrically cooled to -15° C. The SEM stage itself is capable of being cooled over a temperature range of 5 to 300 K. If completely unfiltered, the CCD camera is capable of collecting data of wavelengths from 400 to 1,100 nm. Figure 6 shows the lab setup entirely, Figure 7 shows the stage, and Figure 8 shows the Micro CCD camera attached to the SEM.

Figure 6. JEOL 840A with Cathodoluminescence and Optical Microscope

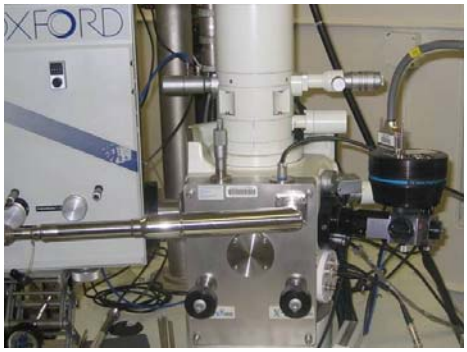

Figure 7. SEM Stage

Figure 8. Micro CCD Camera

This system is used to capture images of drifted and diffused charge. In order to apply an electric field within the SEM, contacts are fixed to the sample. The sample is n-type GaAs with a high purity epitaxial layer doped at N_D-N_A = $5.1x10^{13}$ cm^{-3}. The layer's thickness is approximately 80 μm on top of a semi-insulating substrate. The sample has contacts fixed 1 mm apart. Figure 9 is an image of the top of the sample and contacts taken with an optical microscope.

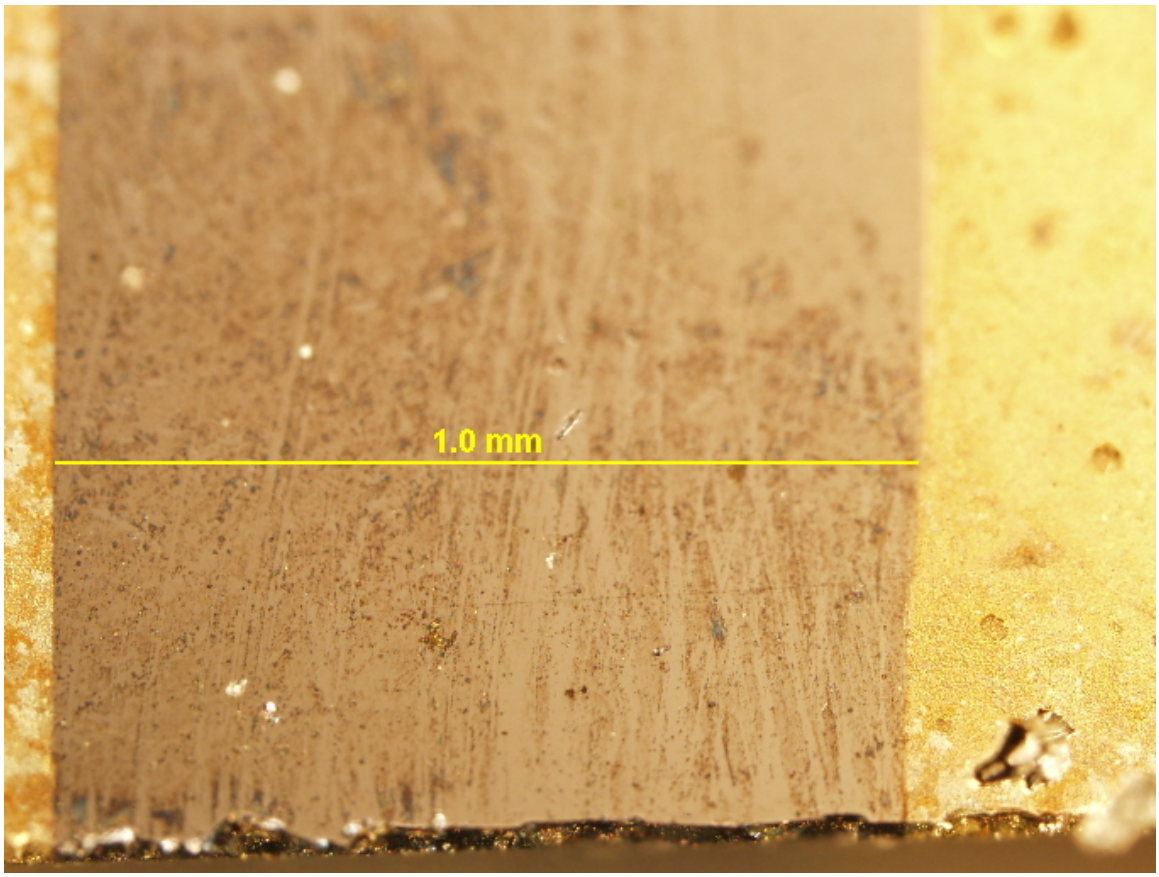

Figure 9. Optical Image of GaAs Sample with Contacts Fixed 1 mm Apart

Using a Keithley source meter, biases ranging from -100 to 100 V are applied across the contacts, creating an electric field in the sample and drifting the charge. Using the SEM in spot mode to generate excess carriers, a series of images are taken of the luminescence resulting from the recombination of the charge. Figure 10 shows images of the recombination distribution as a function of the applied field. Notice that when there is no applied voltage, the charges

experience no net drift. As more voltage is applied, the drift behavior gets gradually more pronounced. In the case that a potential of 100 V is applied, the tail extends to approximately 120 μm. The small spot next to the electron beam spot is an artifact of the microscope where mirrors just barely misaligned cause a reflection in the images. The small spot has no effect on the following analysis and is ignored. The images are 512 by 1024 pixels which corresponds to approximately 205 by 410 μm.

0 V

10 V

20 V

30 V

40 V

50 V

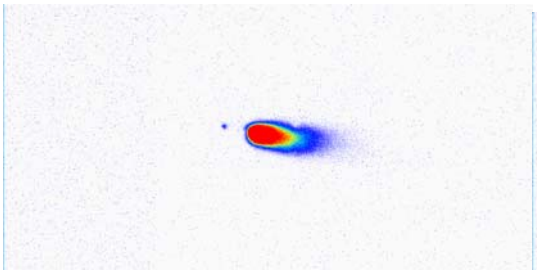

60 V

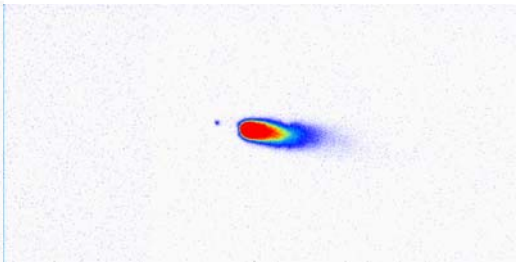

70 V

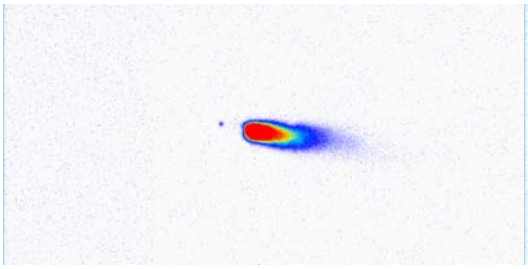

80 V

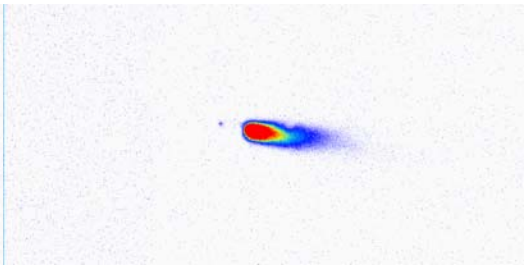

90 V

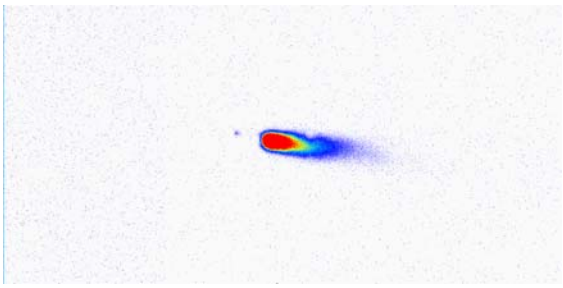

100 V

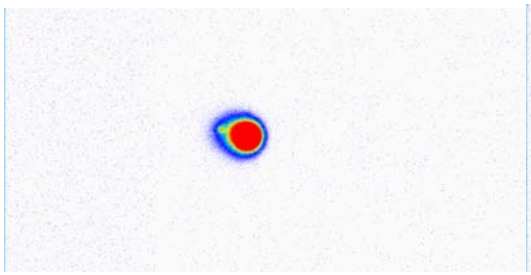

-10 V

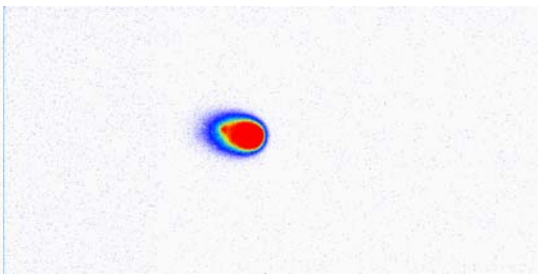

-20 V

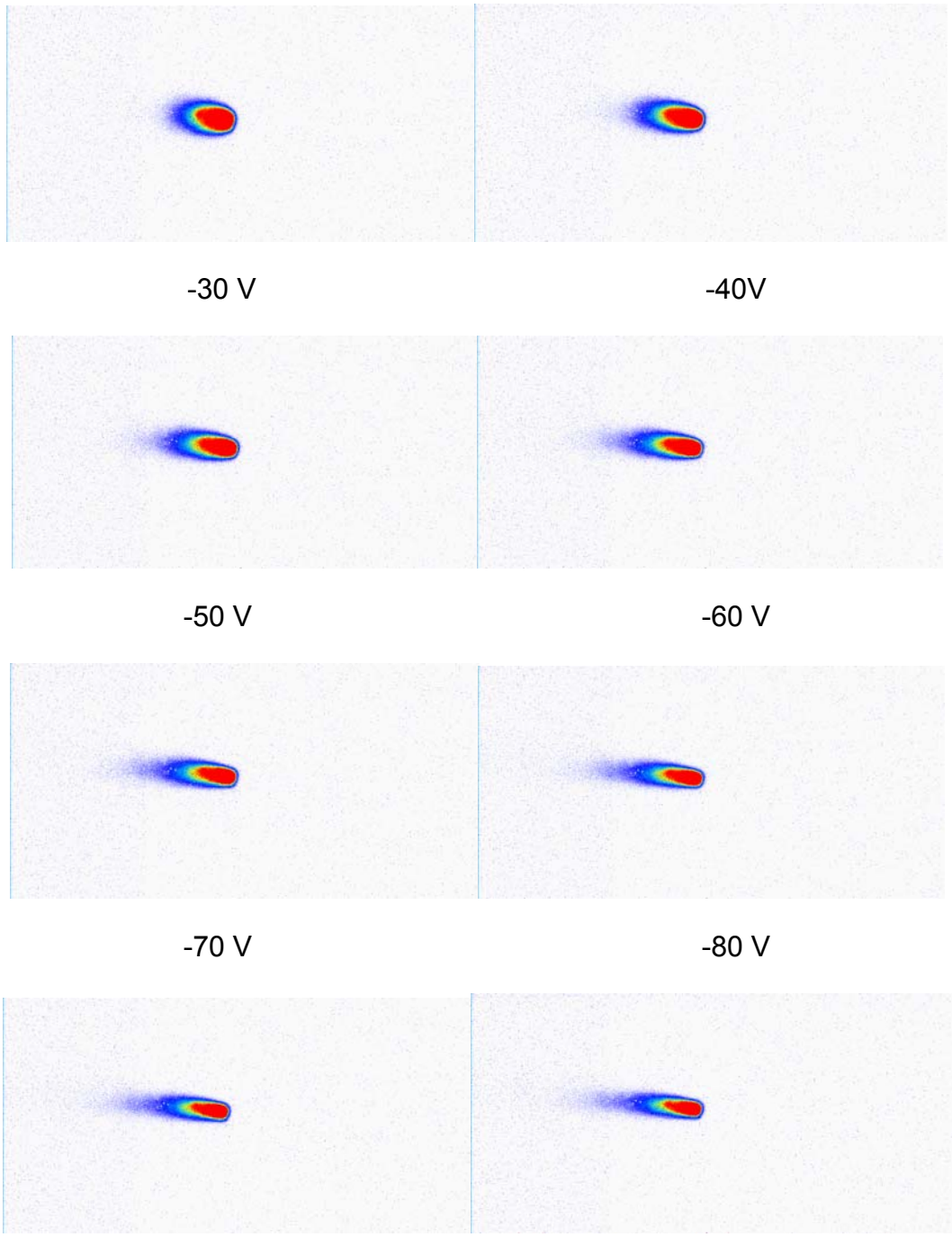

Figure 10. Recombination Luminescence Images as a Function of Applied Field

The intensity distribution is extracted from these images using a Micro CCD software program. The intensity data can be extracted in several different

ways with this program but for the purposes of this thesis only the “line” mode is pertinent. The line mode extracts the intensity across the image from one selected pixel to another selected pixel. In order to accurately measure the intensity of the drifted tail as a function of electric field, the exact same pixel-to-pixel line is drawn across each image. These two pixels were selected in order to produce a line that goes straight through the peak intensity in the direction of drift. Figure 11 shows the micro CCD line used to extract intensity drawn across the 0 V image and the 100 V image to illustrate this point.

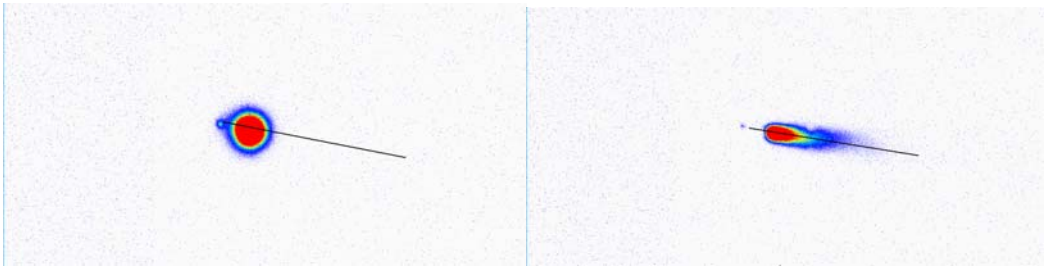

Figure 11. Recombination Luminescence Images with Micro CCD Line for Data Extraction

The line scans of the normalized intensity curves as a function of distance from the electron beam are shown in Figure 12 for the positive applied biases (a) from 0 to 100 V and the negative applied biases (b) from -100 to 0 V.

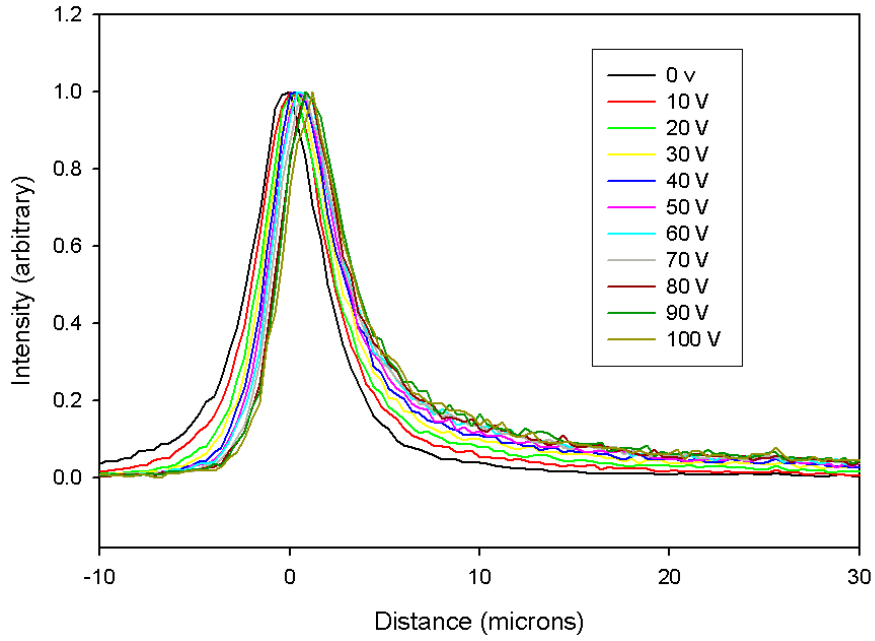

(a) Intensity as a Function of Position for Positive Applied Fields

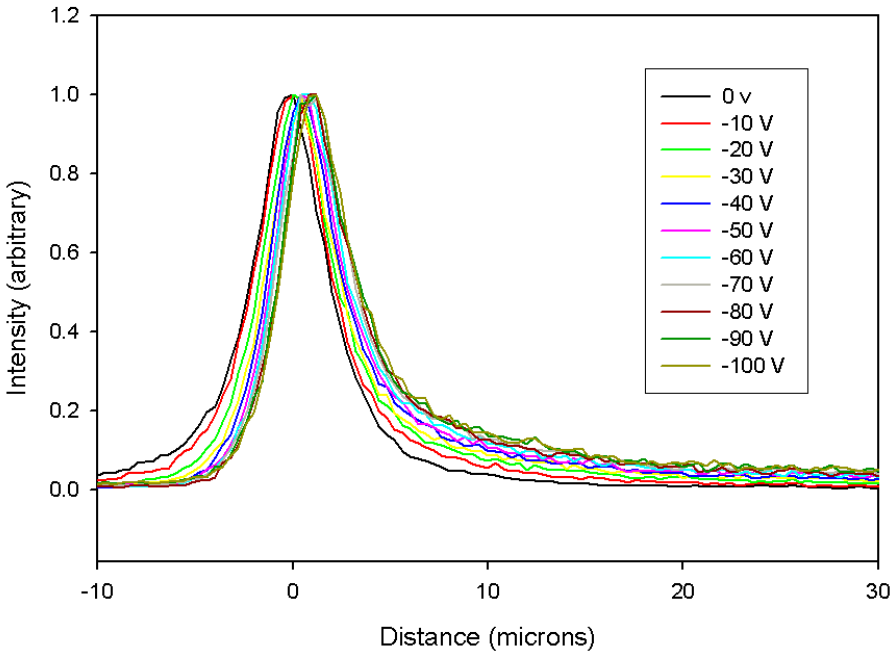

(b) Intensity as a Function of Position for Negative Applied Fields

Figure 12. Normalized Intensity Curves for Positive and Negative Applied E Fields

On a semi-logarithmic plot, the intensity distributions are nearly linear over a certain region which implies that they may be modeled by a simple negative exponential function as discussed in the previous chapter such that:

$$I = \left(\frac{1}{\sqrt{x}}\right) K_o \left(\frac{|x|}{L_{diff}}\right) \square\ e^{Cx}$$

where I is the excess minority carrier density and

$$C = \frac{L_{drift} - \sqrt{L_{drift}^2 + 4L_{diff}^2}}{2L_{diff}^2}$$

$$= \left(\frac{e}{2kT}\right) E - \sqrt{\left(\frac{e}{2kT}\right)^2 E^2 + \frac{1}{L_{diff}^2}}$$

The slopes of the semi-logarithmic curves at a distance of 5 to 20 μm from the center were extracted using a linear regression. Figure 13 shows these slopes along with the original curves for both the positive (a) and negative (b) applied bias. The linear fit is accurate for the positive applied bias with an average error of 10.47%. The linear fit is accurate for the negative applied bias with an average error of 10.52%.

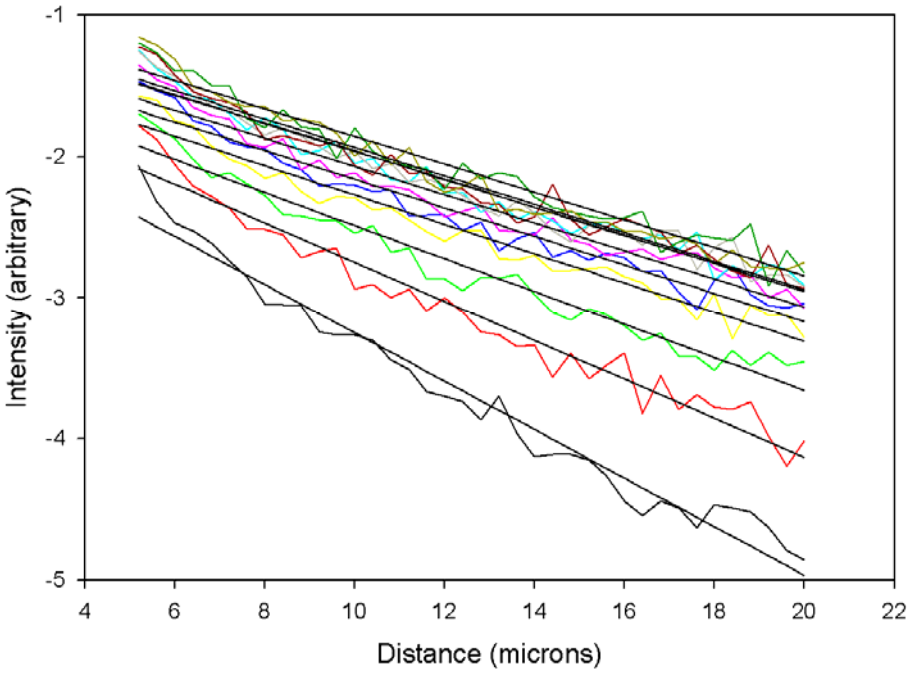

(a) Positive Applied Biases

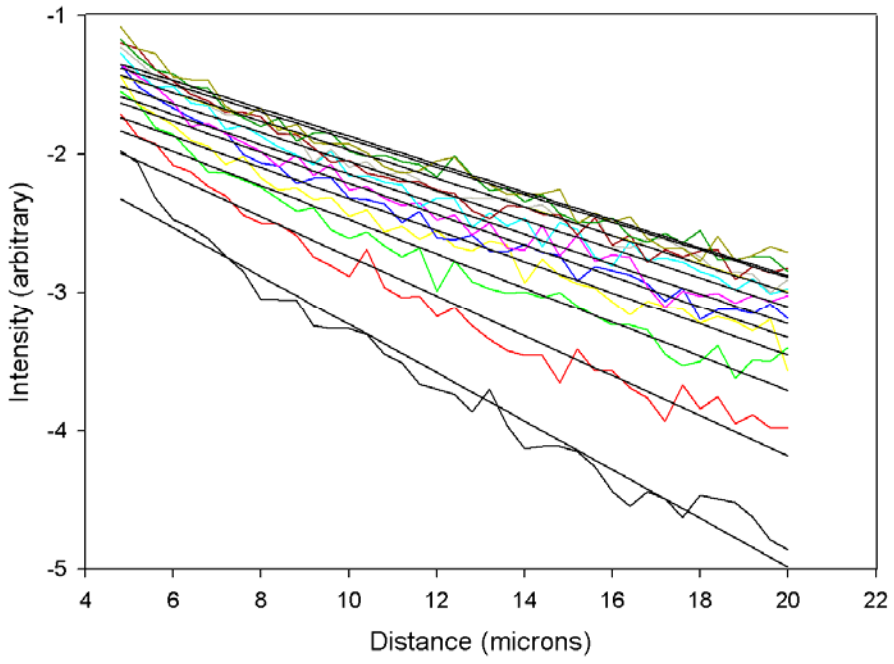

(b) Negative Applied Biases

Figure 13. Linear Regression of Semi-Logarithmic Intensity Curves

After extracting the slope of the semi-logarithmic curve and assuming the applied electric field is known, L_{diff} may be found as:

$$Slope = C = \left(\frac{e}{2kT}\right)E - \sqrt{\left(\frac{e}{2kT}\right)^2 E^2 + \frac{1}{L_{diff}^2}}$$

The $\mu\tau$ product is determined as

$$L_{diff} = \sqrt{D\tau} = \sqrt{\frac{\mu\tau kT}{e}}$$

L_{drift} is calculated given that

$$L_{drift} = \mu\tau E$$

Table 3 shows the final L_{diff}, L_{drift}, and $\mu\tau$ product from the 2D analysis for each applied electric field. Although the sample is thick enough (80 μm) to require a more sophisticated three-dimensional analysis, the two dimensional analysis provides a starting point to asses the effect of diffusion in the 3rd dimension.

Voltage (V)	E Field ($\frac{V}{cm}$)	Slope ($\frac{\text{intensity}}{\mu m}$)	L_{diff} (μm)	L_{drift} (μm)	$\mu\tau$ ($\frac{cm^2}{V}$)
-100	-1000	-0.100	1.57	9.71	9.71×10^{-7}
-90	-900	-0.099	1.66	9.79	1.09×10^{-6}
-80	-800	-0.103	1.73	9.39	1.17×10^{-6}
-70	-700	-0.103	1.85	9.39	1.34×10^{-6}
-60	-600	-0.105	1.97	9.12	1.52×10^{-6}
-50	-500	-0.108	2.11	8.76	1.75×10^{-6}
-40	-400	-0.112	2.30	8.35	2.09×10^{-6}
-30	-300	-0.113	2.62	8.07	2.69×10^{-6}
-20	-200	-0.123	2.98	6.99	3.49×10^{-6}
-10	-100	-0.144	3.59	5.07	5.07×10^{-6}
0	0	-0.172	5.83	0.00	1.34×10^{-5}
10	100	-0.139	3.68	5.34	5.34×10^{-6}
20	200	-0.117	3.08	7.44	3.72×10^{-6}
30	300	-0.104	2.74	8.86	2.95×10^{-6}
40	400	-0.101	2.43	9.29	2.32×10^{-6}
50	500	-0.100	2.21	9.57	1.91×10^{-6}
60	600	-0.100	2.03	9.70	1.62×10^{-6}
70	700	-0.099	1.88	9.71	1.39×10^{-6}
80	800	-0.101	1.75	9.64	1.21×10^{-6}
90	900	-0.098	1.67	9.89	1.10×10^{-6}
100	1000	-0.105	1.53	9.24	9.24×10^{-7}

Table 3. Slope, L_{diff}, L_{drift}, and $\mu\tau$ Product as a Function of Applied Electric Field

B. 3D ANALYSIS OF MOBILITY-LIFETIME PRODUCT IN GALLIUM ARSENIDE

In the 3D case, diffusion from a point source occurs as

$$\left(\frac{1}{|r|}\right)e^{\left(\frac{-r|}{L_{diff}}\right)}$$

where $r=\sqrt{x^2+y^2+z^2}$. Therefore, the diffusion is occurring in 3D but the transport distribution is still collected as 2D images. The 2D image and the 3D diffusion must be related numerically, as they can no longer be related analytically. The Mathcad integration model provides a way to calculate and integrate the 3D diffusion.

The simulation is set to integrate from 0 to 50 μm under the assumption that the charge distribution does not penetrate to significantly greater depths than this in the material. Figure 14 is the penetration depth graph for the original distribution of charge in GaAs as a function of the energy of the incident electron beam. At 20 kV the penetration depth is 5.13 μm.

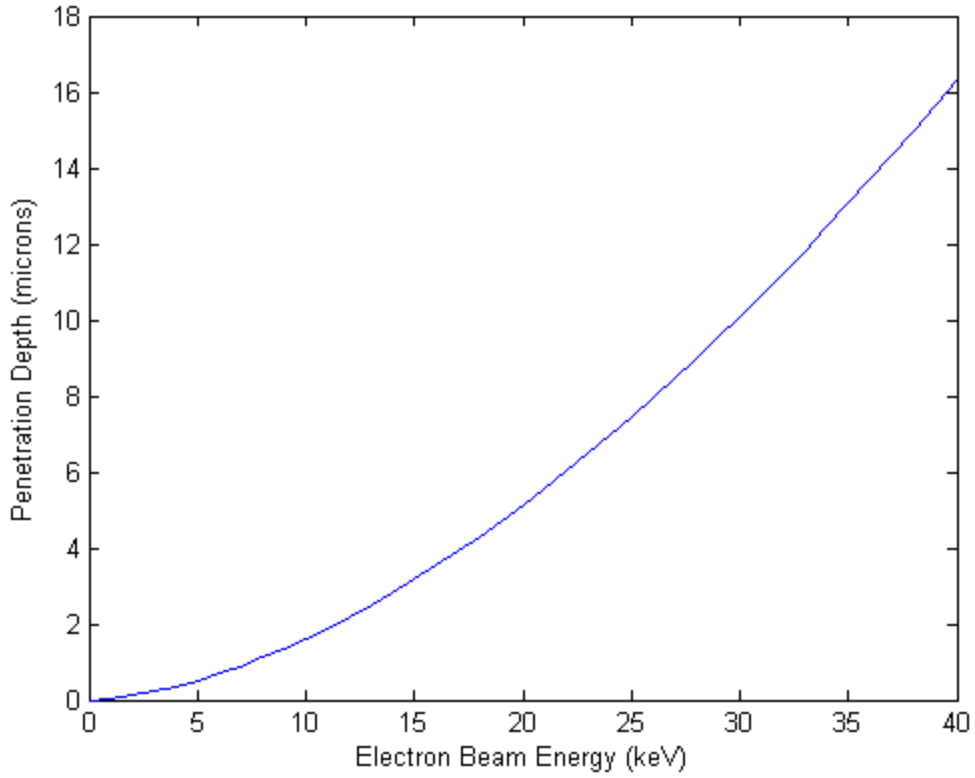

Figure 14. Penetration Depth Charge Generation in GaAs as a Function of the Incident Electron Energy

The simulation requires that one inputs an applied electric field and diffusion length and then generates an intensity output as a function of distance from the center. Thus, the simulation produces an intensity versus distance curve similar to the one extracted from the transport image in the 2D case. Figure 15 illustrates how integrating through more layers of the material (e.g. for higher values of D) affects the simulation. Integrating through more layers accounts for more recombination luminescence within the sample and results in a higher intensity.

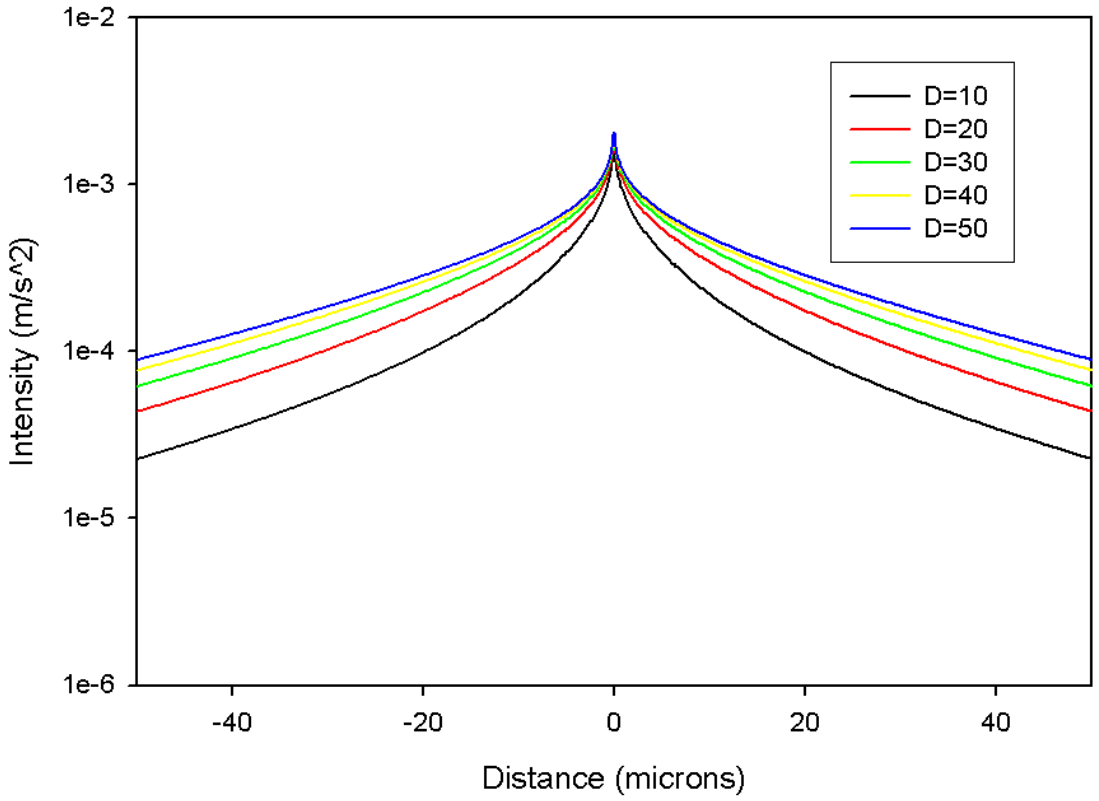

Figure 15. Mathcad Simulation for L=50 μm Integrated with D=10, 20, 30, 40, and 50 μm

Figure 16 shows the same simulation except the diffusion length was set to 5 μm rather than 50 μm. Since the diffusion length is smaller, recombination does not occur in as many layers in the material. Therefore, the difference between integrating through 10 μm versus integrating through 5 μm is minimal especially when compared to Figure 15. If a material has a greater diffusion length, more recombination can occur at greater distance from the surface and integrating to sufficient depth is crucial.

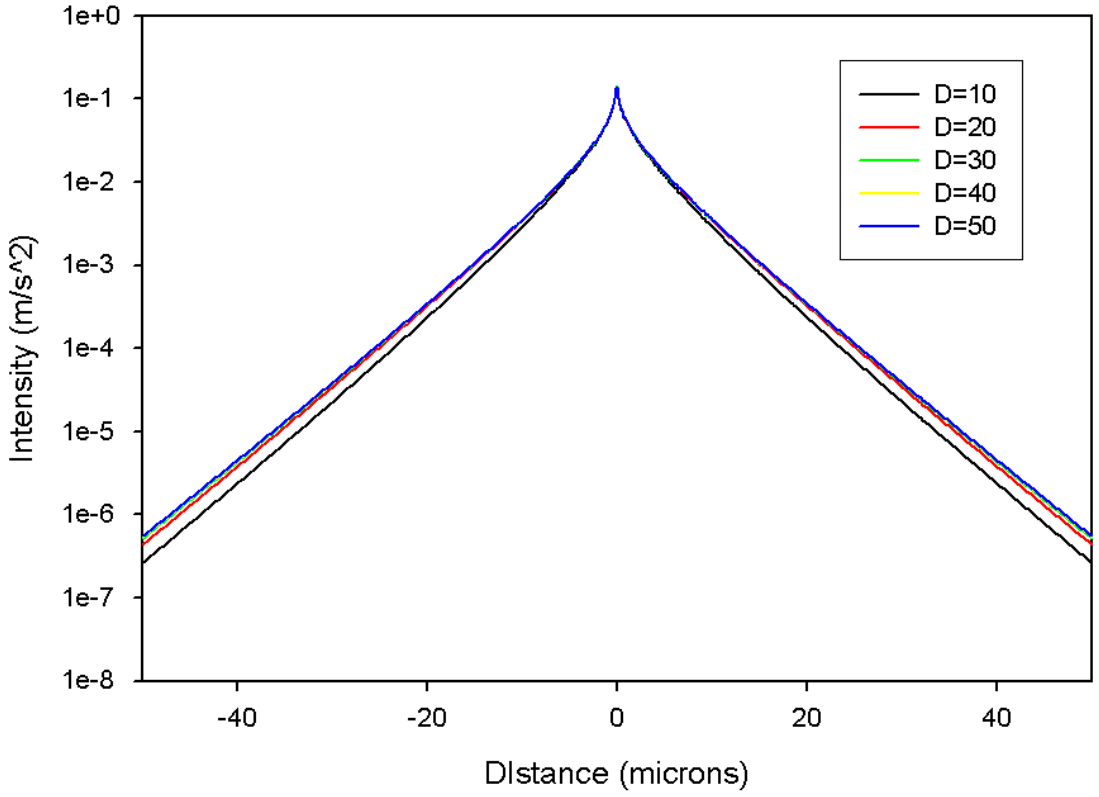

Figure 16. Mathcad Simulation for L=5 μm Integrated with D=10, 20, 30, 40, and 50 μm

The 3D diffusion simulation with drift was run for each 10-volt increment from -100 to 100 V for a range of diffusion lengths from 0 to 10 μm. The slopes of the simulated semi-logarithmic curves at a distance of 5 to 20 μm from the center were extracted using a linear regression. Figure 17 shows these slopes along with the original curves for positive applied bias extracted for D=50 μm. The linear fit is accurate for the positive applied bias with an average error of 2.36%.

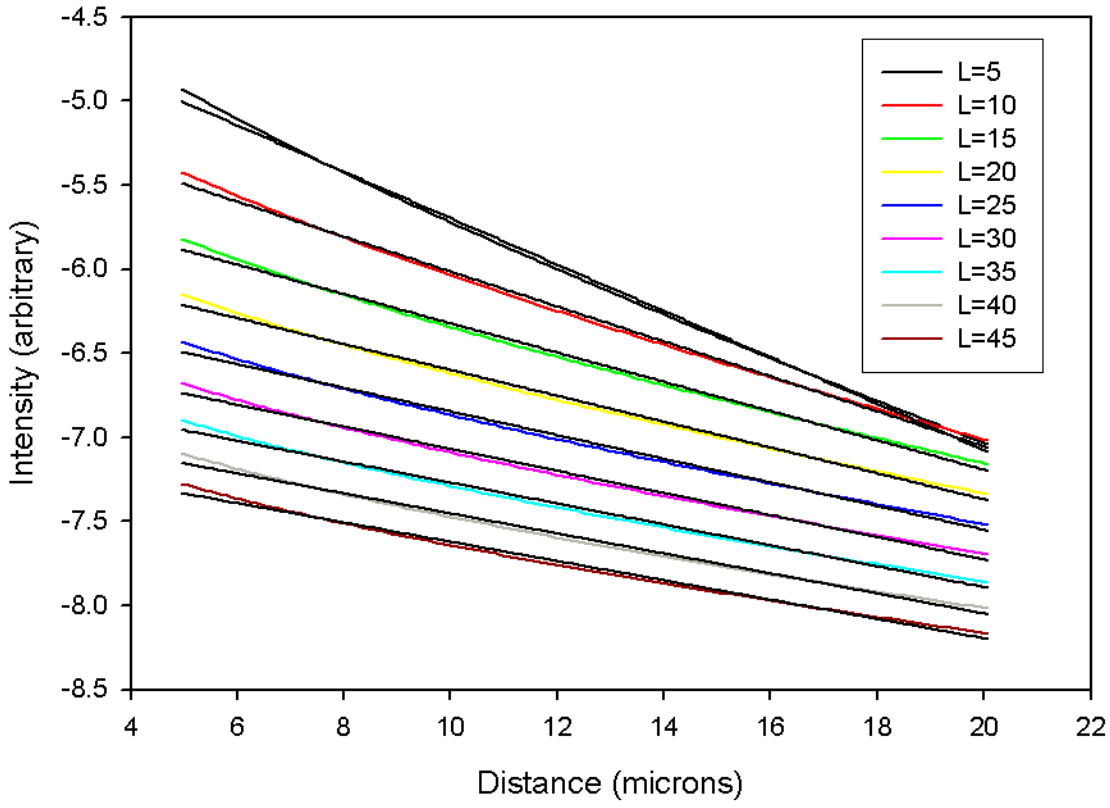

Figure 17. Linear Regression to Approximate Slope When D=50 μm for a Range of Diffusion Lengths from 5 to 45 μm

The diffusion length is then graphed as a function of slope. Therefore, the experimental slope extracted directly from the transport images are used to find the estimated diffusion length for the material for a specified applied electric field. Figure 18 shows the diffusion length as a function of slope for each applied voltage.

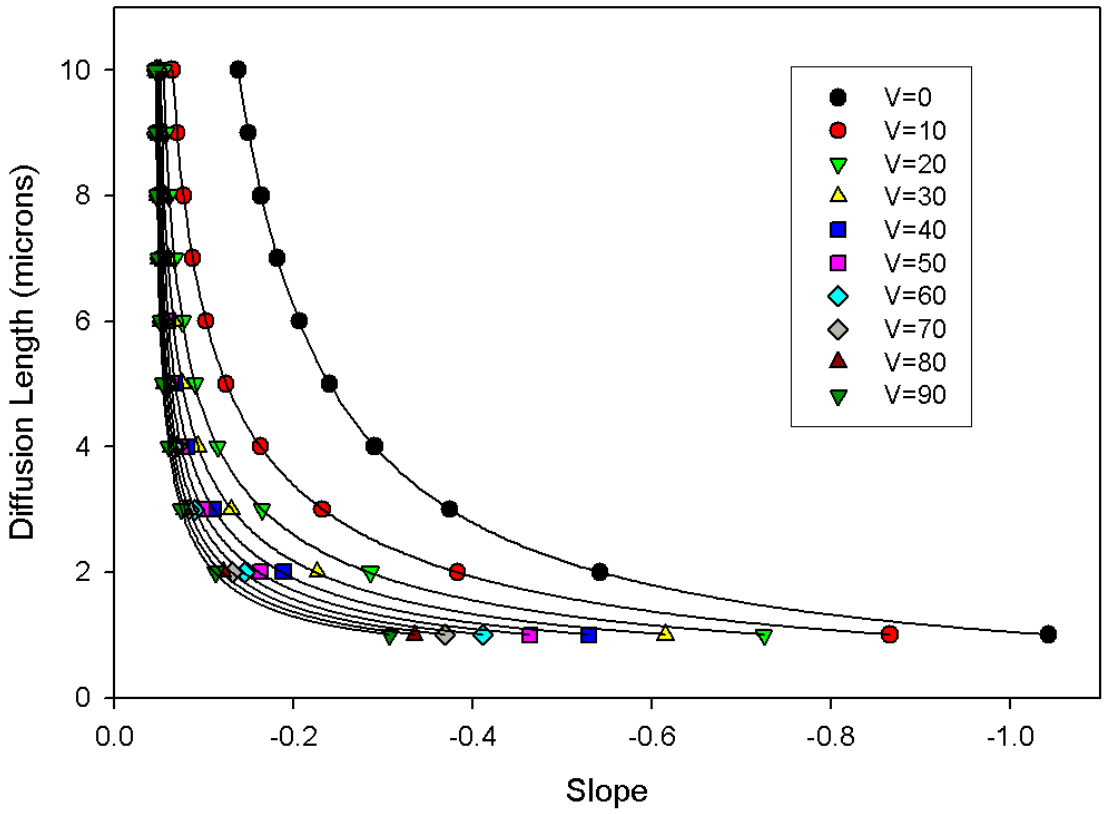

Figure 18. Simulated Diffusion Length as a Function of Slope for Electric Fields from 0 to 90 V/mm

Once L_{diff} is found, the $\mu\tau$ product and L_{drift} can be calculated as previously shown. Table 4 gives the final values of this analysis for each applied voltage.

Voltage (V)	E Field ($\frac{V}{cm}$)	Slope ($\frac{\text{intensity}}{\mu m}$)	L_{diff} (μm)	L_{drift} (μm)	$\mu\tau$ ($\frac{cm^2}{V}$)
0	0	-0.172	7.53	0.00	2.23 x10^{-5}
10	100	-0.139	4.57	8.23	8.23 x10^{-6}
20	200	-0.117	3.94	12.20	6.10 x10^{-6}
30	300	-0.104	3.63	15.56	5.19 x10^{-6}
40	400	-0.101	3.25	16.63	4.16 x10^{-6}
50	500	-0.100	2.97	17.29	3.46 x10^{-6}
60	600	-0.100	2.73	17.58	2.93 x10^{-6}
70	700	-0.099	2.52	17.44	2.49 x10^{-6}
80	800	-0.101	2.33	17.10	2.14 x10^{-6}
90	900	-0.098	2.24	17.75	1.97 x10^{-6}

Table 4. L_{diff}, L_{drift}, and $\mu\tau$ Product for Each Applied Electric Field

The extracted diffusion length for the 0 V applied bias case is 7.5 μm. This value is significantly less than expected for high purity GaAs grown by the liquid phase epitaxy technique. In the Australian Journal of Physics, Butcher *et al.* measure the minority carrier diffusion lengths using an electron beam induced current (EBIC) technique. They report that the diffusion length of their liquid phase epitaxy (LPE) n-type GaAs doped at 10^{14} cm^{-3} is 250 μm [13].

One experimental challenge is that the electric field must be accurately known. Potentially, in a two contact measurement, the electric field can be much lower than assumed. The bias is applied across metal contacts deposited on the surface of the sample. If the contacts aren't perfectly ohmic, a voltage drop may

occur between the contacts and the sample. Therefore, the amount of applied voltage across the contacts is not the actual amount of voltage creating the electric field in the material. For example, if there is a 2 V drop across both of the contacts and 10 V are applied across the sample, only 6 V are actually available to induce an electric field between the contacts. The potential barrier between the metal contacts and the semiconductor is known as the Schottky barrier and is frequently used advantageously in diodes. In this case, however, the Schottky barrier may be a source of error.

Designing a sample with four contacts instead of two can mitigate the Schottky barrier effect in this technique. Applying a voltage across the outer two contacts and measuring the voltage across the inner two contacts ensures that the electric field is accurately known. Figure 19 is a schematic top view of the sample and four point contact geometry.

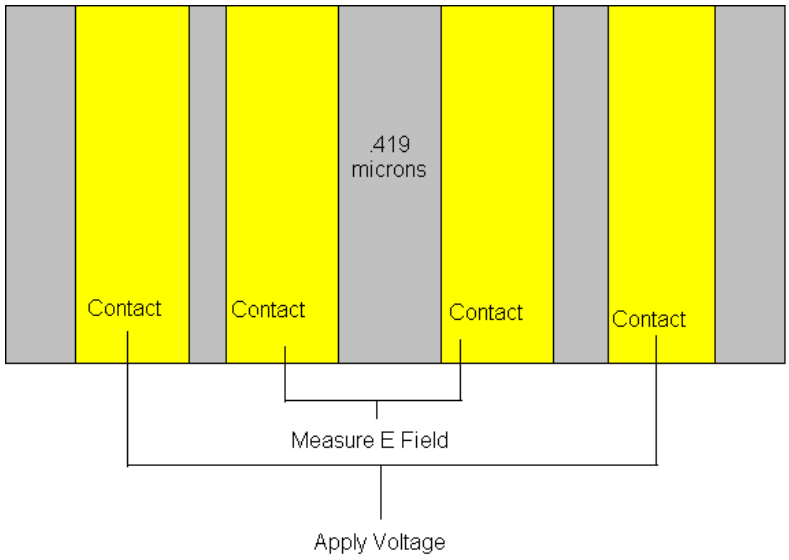

Figure 19. Schematic of Sample with Four Point Contact Geometry

An n-type GaAs sample doped at 10^{14} cm^{-3} grown by molecular beam epitaxy on a semi-insulating substrate was obtained from Lawrence Berkeley National Laboratory. The sample has four ohmic NiGeAu contacts. The inner

contact distance is 419 μm. Current was applied to the outer contacts and the voltage drop across the inner contacts was measured. Figure 20 is the IV curve of the 4 point contact illustrating the drop from the outer contacts to the inner contacts.

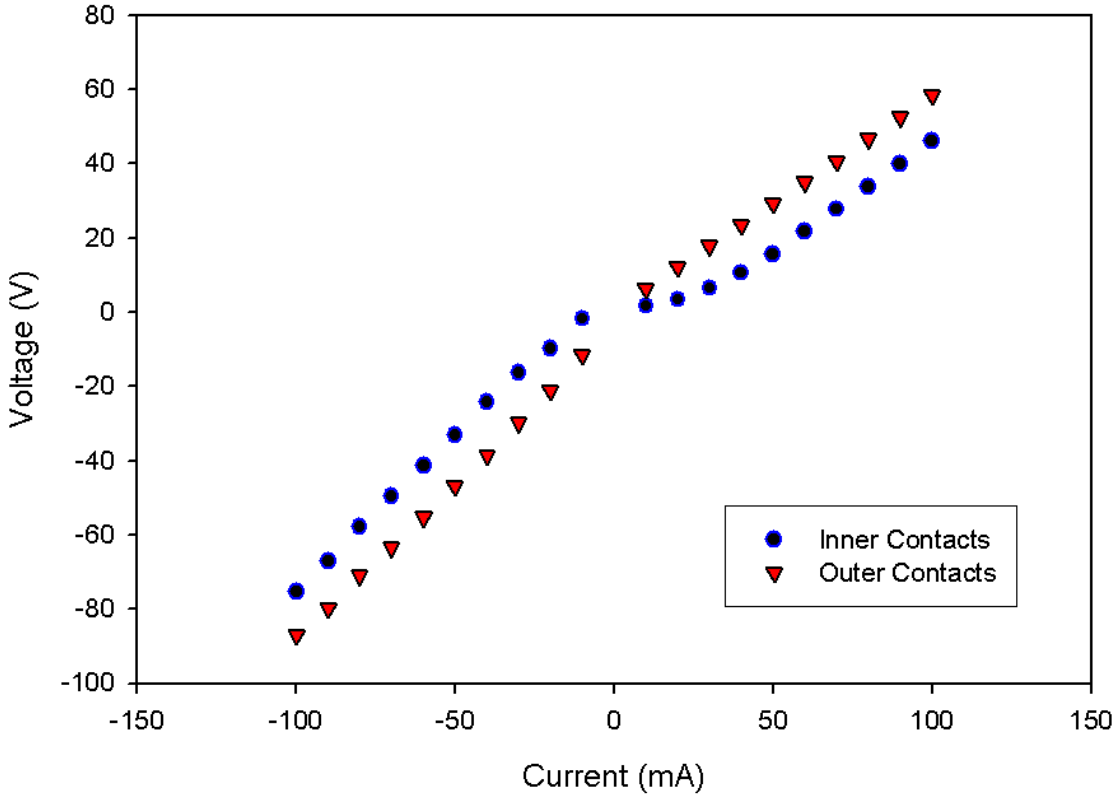

Figure 20. IV Curve Measured at Inner and Outer Contacts on 4 Point Sample

The average voltage drop at the contacts is consistently about 12.12 V regardless of the magnitude of the applied voltage or current across the outer contact. The diffusion length, however, hardly changes for voltages exceeding 40 V. If the Schottky barrier were the primary source of the error in the technique, the L_{diff} term should still be much larger and should increase with voltage linearly, as the voltage drop due to contact effects does not increase with field.

The transport imaging technique was used on this 4 point contact sample. Figure 21 shows the images of the recombination luminescence based on the applied field. The diffusion length of holes for this sample is much shorter than the diffusion length for the material previously used. This difference is most likely due to the hole lifetime in the material and not to the contacts The horizontal length of each of the images below is 235 μm.

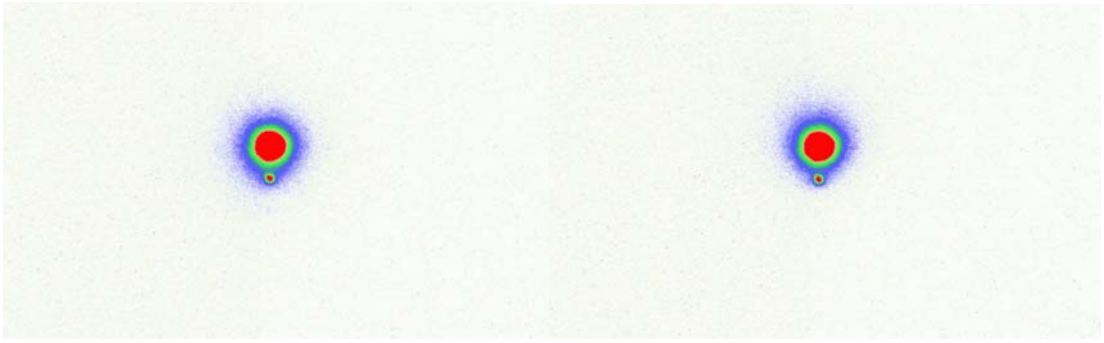

0 mA 10mA

20 mA 30 mA

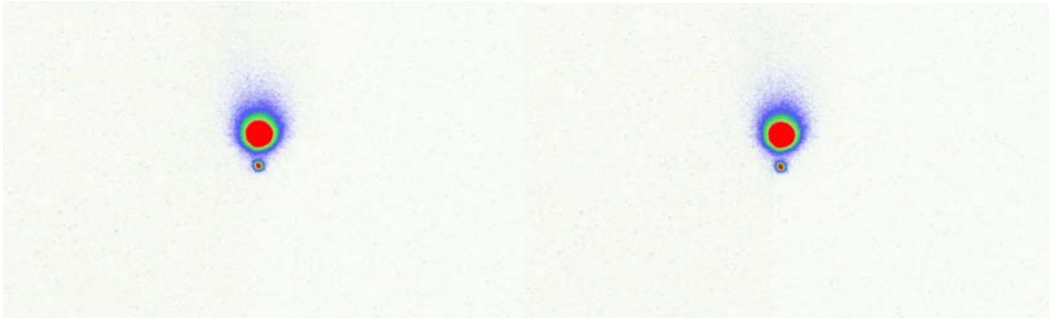

40 mA 50mA

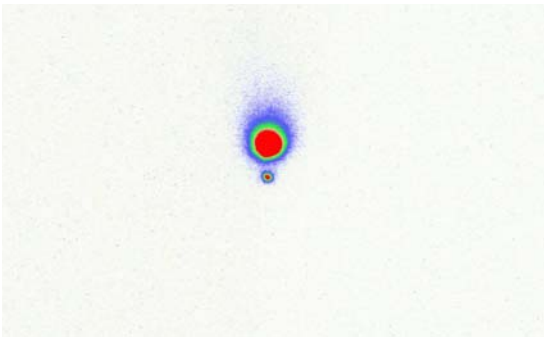

60mA

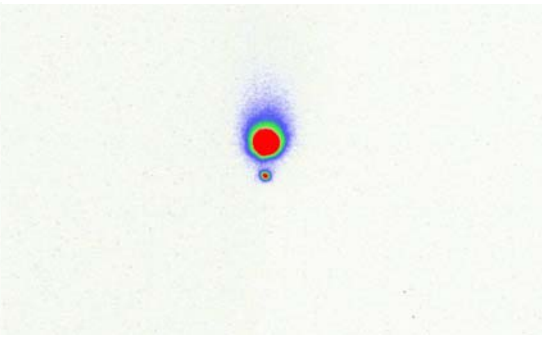

70mA

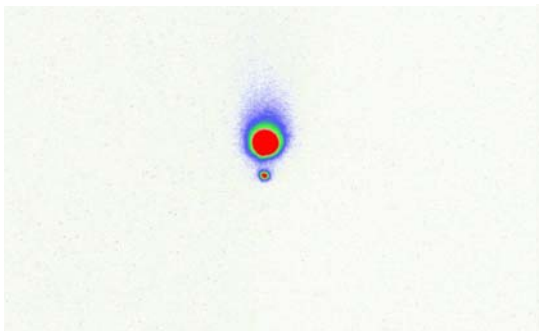

80mA

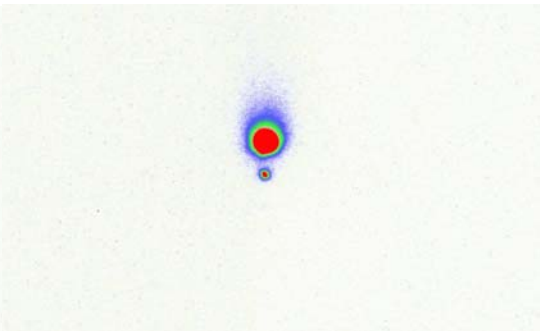

90mA

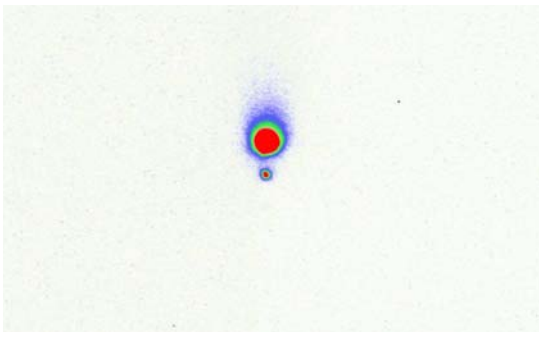

100 mA

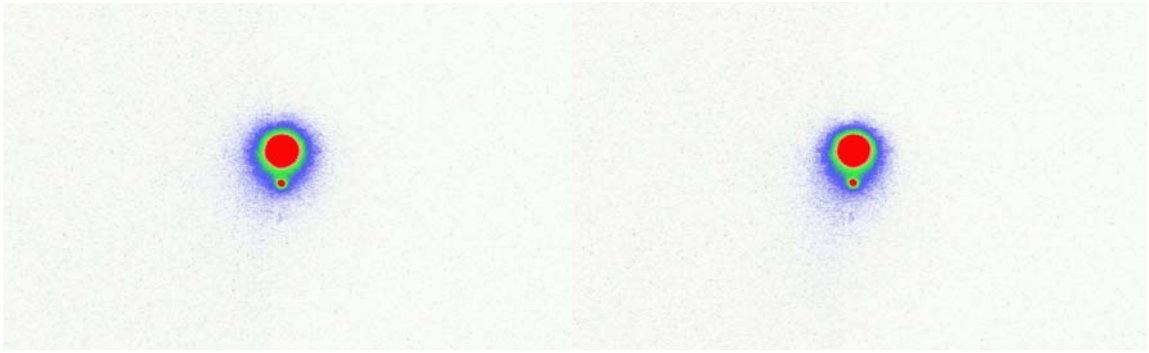

-10 mA

-20 mA

-30 mA

-40 mA

-50 mA

-60 mA

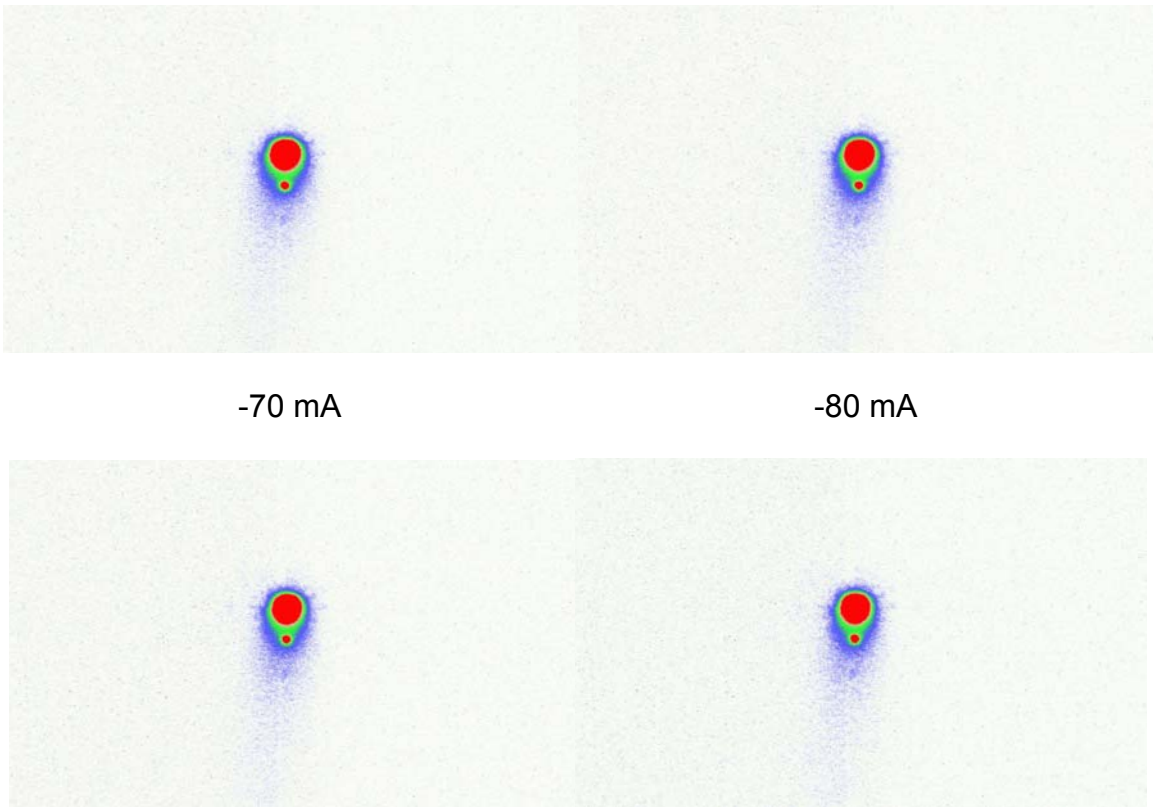

Figure 21. Recombination Luminescence as a Function of Applied Current

Analysis of the 0 V case was performed. For the four point contact sample, Figure 22 shows the collection of curves for normalized intensity as a function of distance from the incident beam and Figure 23 is the semi-logarithmic graph with the linear regression performed to determine slope for the 0 V case. The slope for the 0 V case is determined to be -0.3602 and, therefore, L_{diff} is calculated to be 2.8 μm. This value is small compared to the 5.8 μm in the previous analysis. The smaller diffusion length is indicative of different techniques used to grow the materials at Lawrence Berkeley National Laboratory.

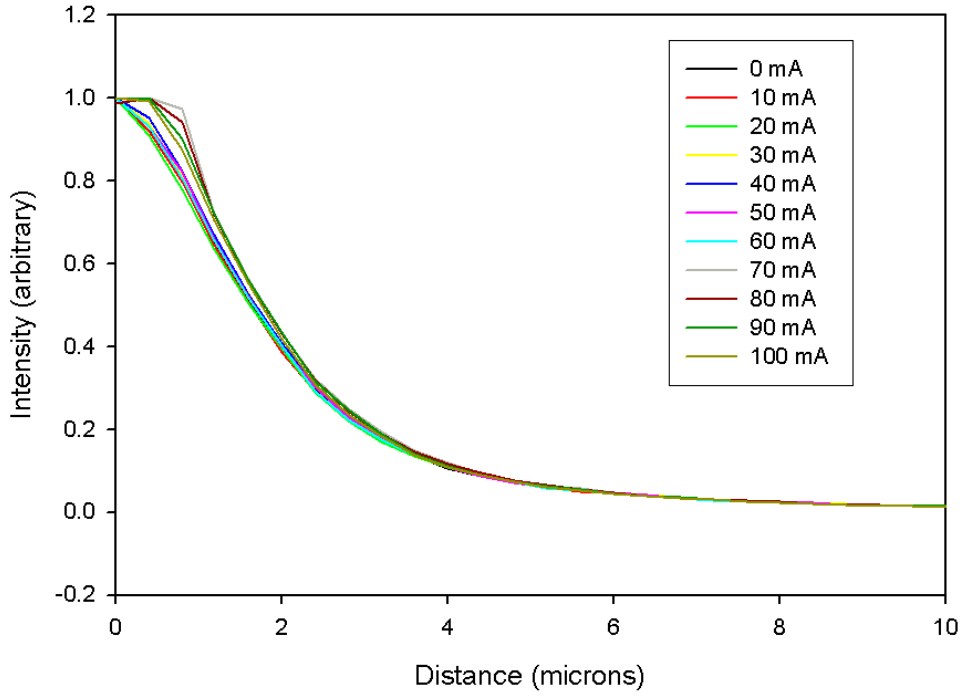

Figure 22. Intensity as a Function of Distance for 4 Point Sample

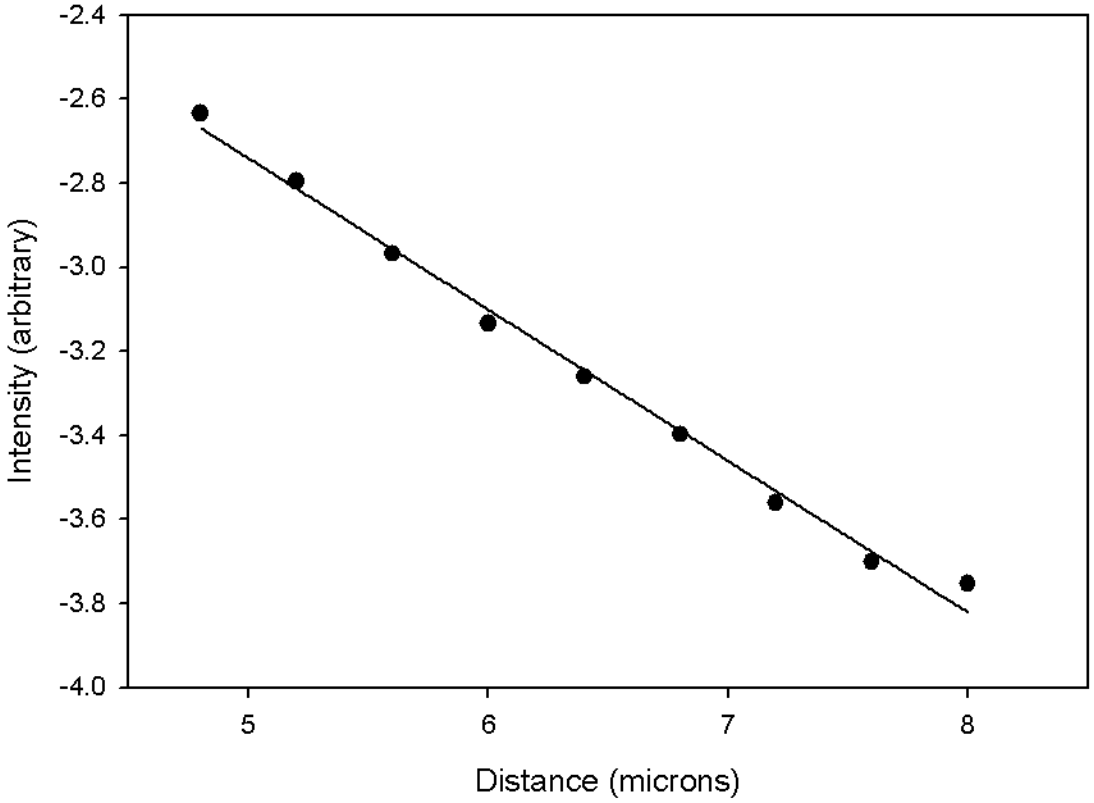

Figure 23. Linear Regression to Determine Slope for Four Point Sample in the Absence of an Applied Field

Another limitation in the analysis is most likely associated with surface recombination effects. These samples have a free surface that acts as a sink for charge carriers. When recombination occurs at a semiconductor surface, there is a flow of charge carriers towards the surface and a conventional flow of current away from the surface [14]. Excess carriers recombine immediately after reaching the surface if the surface state density is very large. Therefore, the material actually has a much longer diffusion length, drift length, and $\mu\tau$ product then the transport image indicates as the tail of the drifted charge under bias is severely reduced by the surface recombination.

In order to account for this effect, a surface recombination velocity (S), which arises from a boundary condition for recombination at the surface, must be determined. Chris Frenzen and Clyde Scandrett in the Mathematics Department at Naval Postgraduate School have collaborated on an initial approach to this problem. Using Eigenfunction approximations, a first estimate of S in the 0 V applied bias case has been determined. The diffusion length calculated in the transport imaging technique could be considered the effective diffusion length including the surface recombination effect. The effective diffusion length may be modeled as:

$$\frac{1}{L_{eff}} = \sqrt{\lambda + \frac{1}{L^2} + \left(\frac{\mu E}{2D}\right)^2}$$

where L is the theoretical diffusion length, D is the diffusivity, L_{eff} is the experimental diffusion length, and λ is a term that involves the surface recombination. The above equation is used to solve for λ.

$$\lambda = \xi^2 \qquad \text{and} \qquad \tan(\xi H) = \frac{1}{\xi d_{top}}$$

where d_{top} is defined as $\frac{D}{S}$ and H is the thickness of the material. Assume the thickness is 80 μm. The flux out of the bottom of the sample is ignored under the assumption that the sample is thick enough that there is no surface recombination effect on the bottom side. Upon solving for d_{top}, the surface recombination velocity is then calculated:

$$\frac{1}{d_{top}} = \frac{S}{D}$$

Assume the theoretical diffusion length is $L = 100$ μm and the experimental diffusion length is L_{eff} =8 μm. For the 0 V case, S= 6117 cm/s. This is a realistic value for S and will be a starting point for further analysis with the addition of external field.

These optical techniques for the direct determination of the minority carrier diffusion length and $\mu\tau$ product are being developed to help analyze new materials more readily. The techniques are being tested on well known materials, such as GaAs, to asses their accuracy. In the future, they could be applied to a wide range of new materials to rapidly assess they suitability for use in nuclear radiation detectors requiring a minimum value of $\mu\tau$.

VI. CATHODOLUMINESCENCE OF BISMUTH FERRITE

In parallel with developing optical techniques to analyze semiconductor transport properties, new complex oxides are being explored for possible use in the next generation radiation detectors. One such complex oxide is bismuth ferrite. $BiFeO_3$ (BFO) was identified as a potential candidate and a material of interest because it is high Z, shows simultaneously ferroelectric and magnetic properties and may have a band gap suitable to the application (2-3 eV). The CL of BFO is explored to help characterize the material and determine if it could be a future candidate for optical measurement of $\mu\tau$.

Two sets of samples were obtained from Prof R. Ramesh's research group in the Department of Materials Science and Engineering at UC Berkley. The first set contained two samples. Both samples were lanthanum doped BFO. CYE-5 was grown directly on $DyScO_3$ (110) substrate to get 109 degree domain walls and CYE-010 was grown on a $SrRuO_3$/ $DyScO_3$ (110) substrate to get 71 degree domain walls. The $SrRuO_3$ is a metallic film that acts as a bottom electrode. The BFO films appear very shiny and are approximately 100 nm thick. The $SrRuO_3$ layer on the one sample is between 30 to 50 nm thick and the substrate is approximately 0.5 mm thick.

While taking CL measurements, copper tape is fixed to the samples' surface in an effort to ground the samples as they charge intensely. Materials that are insulating hold charge in the SEM and are hard to focus. The copper tape ameliorates but does not completely correct this problem. The SEM is an intricate and sensitive piece of machinery. Optimizing the internal optical system is crucial. For example, adjusting the stage height by only a few microns can increase the efficiency such that 30% more photons are collected. Spectroscopy was performed on the samples at incident electron beam

intensities ranging from 2 to 20 keV. Figure 24 shows the intensity of the emission as a function of wavelength of CYE-5 taken with a probe current of 1 x 10^{-9} A and a 20 keV electron beam at 2000X magnification.

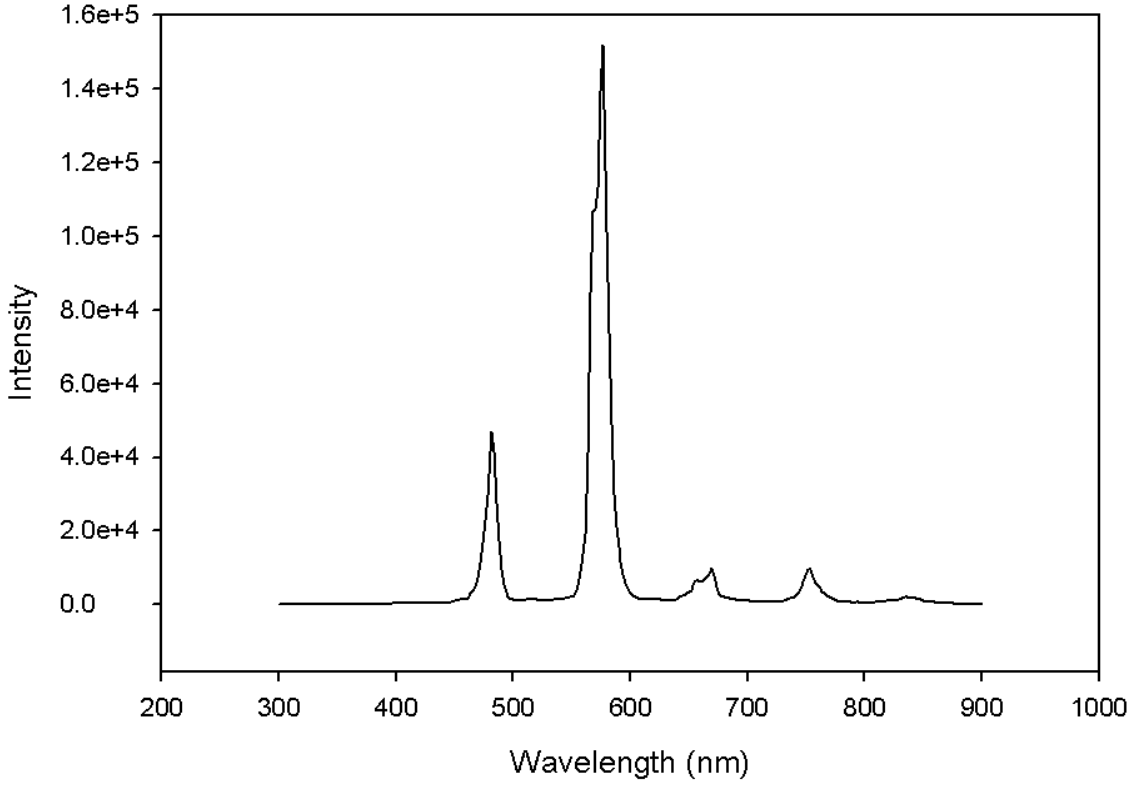

Figure 24. CL of CYE-5 with 1 x 10^{-9} A Probe Current, 20 keV E Beam, and 2000X Magnification

Note the intensity spikes that occur at 482, 576, 670, and 754 nm. These peaks, in particular the 576 nm peak, are so intense they dwarf any subtle material fluctuations in the spectra and are present in the spectra for both CYE-5 and CYE-010 at room temperature for all electron beam intensities ranging from 5 to 20 keV. Reducing the electron beam intensity to 5 keV can help bring out more data from the material. However, at low electron beam intensities, the data is often dominated by noise. One solution is to cryogenically cool the SEM's stage in order to potentially increase radiative recombination in the material.

A modified, liquid helium-cooled stage can be implemented to observe luminescence for temperatures ~5 K. Figure 25 shows the luminescence of CYE-5 cooled to 4.6 K with a magnification at 5000X. The electron beam intensity is 5 keV and the probe current is $3x10^{-9}$ A. The four peaks are still dominant in the luminescence.

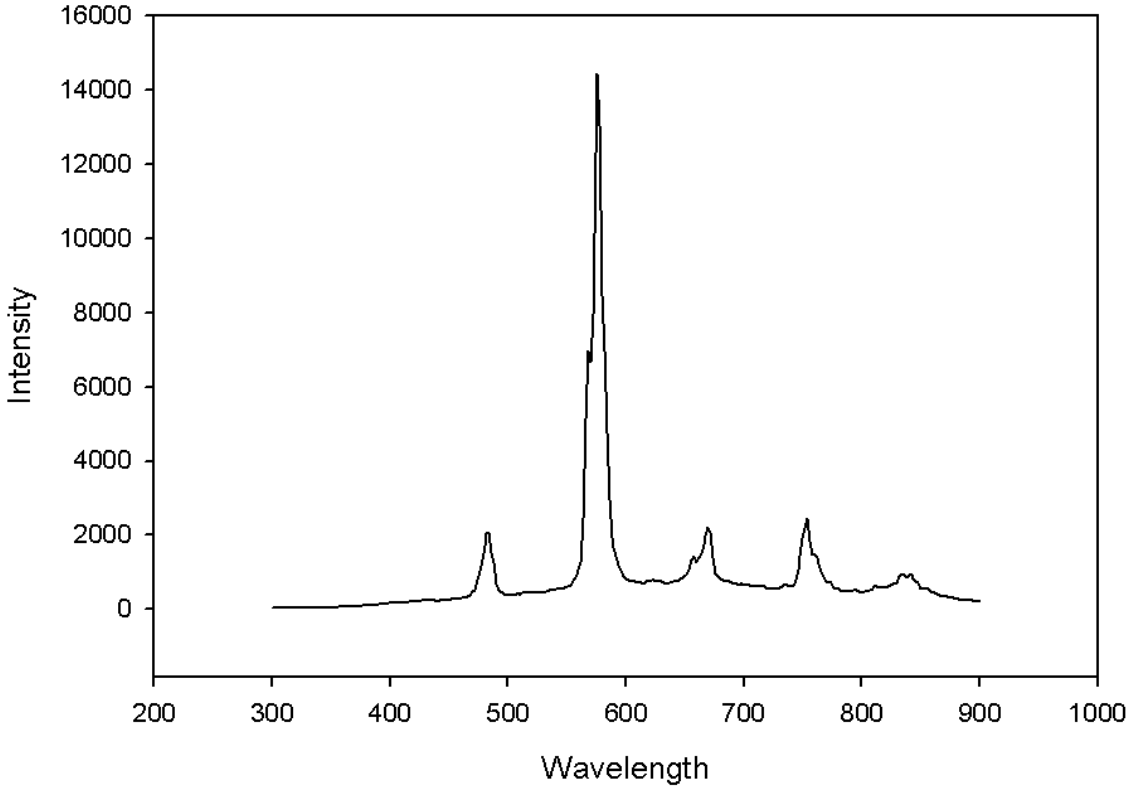

Figure 25. CL of CYE-5 with 3 x 10^{-9} A Probe Current, 5 keV E Beam, and 5000X Magnification at 4.6 K

These four peaks were still dominant in almost all of the collected spectra. The BFO film on these samples is only 100 nm and the incident electrons penetrate to the substrate material. Spectroscopy was performed on the substrate of the sample. Figure 26 shows the luminescence of the substrate as a

function of wavelength. The spectroscopy was performed at 5000X magnification with an electron beam intensity of 20 keV and probe current of $3x10^{-9}$ A.

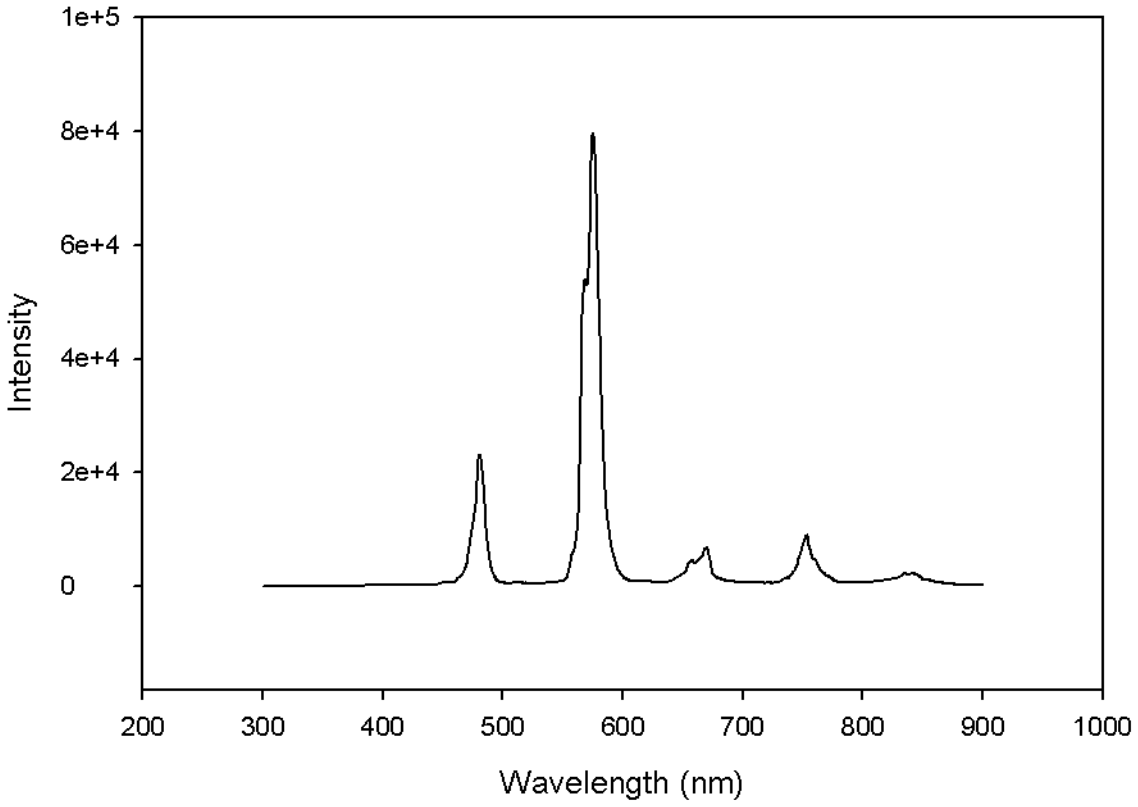

Figure 26. CL of Substrate with 3 x 10^{-9} A Probe Current , 20 keV E Beam, and 5000X Magnification

The four peaks at 482, 576, 670, and 754 nm wavelengths are even more prevalent on the substrate side of the sample. These peaks in luminescence are clearly emissions from the thick $DyScO_3$ substrate rather than the thin BFO layer. Kawai *et al.* reported strong visible CL from dysprosium ions at 480, 575, 660, and 750 nm in Dy-ion-implanted 4H-SiC [15]. This intense luminescence from dysprosium ions aligns almost perfectly with the peaks seen in bismuth ferrite samples grown on dysprosium scandate.

Lawrence Berkeley National Laboratory provided another set of samples with a thicker layer of BFO so that the layer would not be so easily penetrated by the electron beam. This sample consisted of lanthanum doped BFO grown directly on $DyScO_3$ (110) substrate to get 109 degree domain walls. However, instead of a BFO layer that is only 100 nm thick, this sample's BFO layer is 1 μm thick.

CL was performed on the sample at a magnification of 2000X at 10, 20 and 30 keV electron beam intensities with a probe current ranging from $6x10^{-10}$ to $1x10^{-9}$ A. To ensure the equipment was properly operating, bulk GaAs, which has a well know CL spectra, was tested in the same set of experiments as the BFO sample. The bulk GaAs's CL exhibited a peak at 850 nm that is characteristic of the materials 1.4 eV band gap. This result verifies that the equipment was properly functioning.

The substrate's spectrum was taken once again to compare with the film. Figure 27 shows the CL of BFO and the substrate under the same conditions. The magnification was 2000X, the electron beam's intensity was 30 keV, and the probe current was $1x10^{-9}$ A.

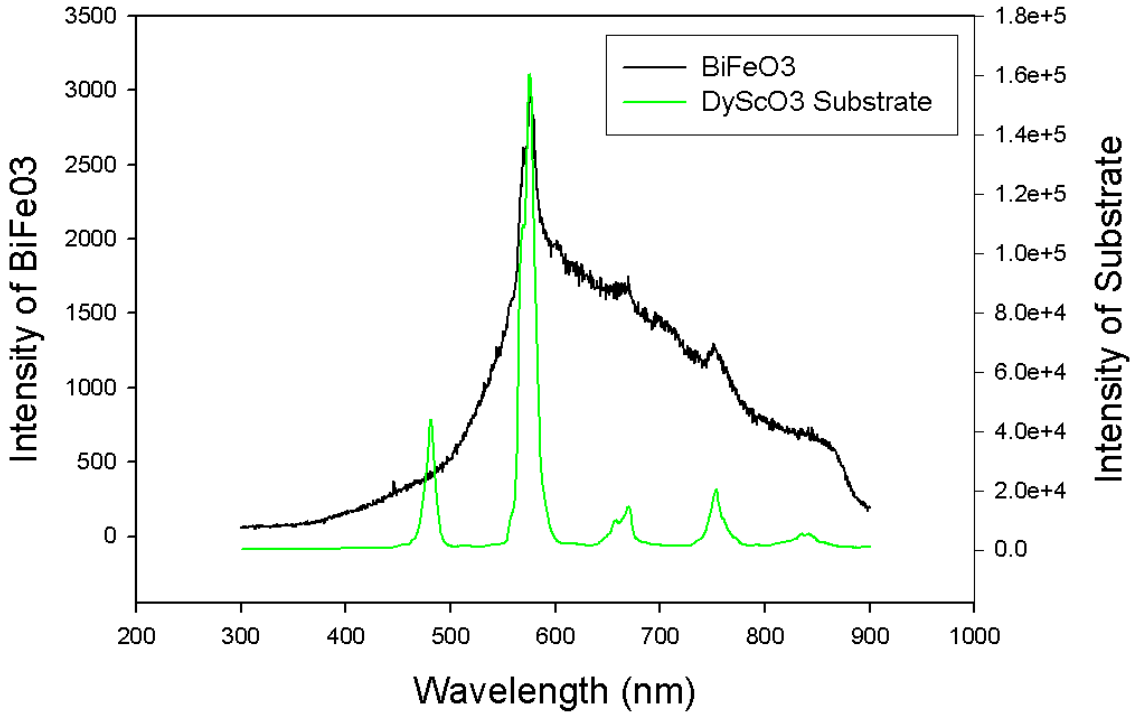

Figure 27. CL on BFO and $DyScO_3$ Substrate with $1x10^{-9}$ A Probe Current, 30 keV E Beam, and 2000X Magnification

The peaks at 576, 670, and 754 nm are still evident in both curves. However, the 480 nm peak is no longer present in the CL spectra for BFO. The absence of the expected luminescence at 480 nm indicates that there is an optical absorption occurring in BFO somewhere between 480 and 576 nm or, equivalently, between 2.15 and 2.58 eV. This corresponds with the values suggested for the band gap in published literature. Basu et al. examined the optical properties and photoconductivity of thin films of BFO. They report that absorption is evident at beginning at 2.5 eV and that there is an optical absorption onset near 2.17 eV [16].

Further research is needed to investigate thicker films and materials variations that may enhance luminescence. Material luminescence may depend on temperature, doping, or the way a material is grown. For instance, doping the material differently can improve conductivity. As a result, transport imaging may

be used to analyze BFO under the right conditions. Additional research is required to optimize the materials so that transport imaging techniques can be used to characterize their electrical transport properties.

THIS PAGE INTENTIONALLY LEFT BLANK

VII. CONCLUSIONS AND FUTURE RESEARCH

Nuclear terrorism is an on-going international security threat that has created a critical need for inexpensive, room temperature devices that can detect gamma rays. In order to rapidly characterize materials that could potentially be used in these detectors, an optical technique has been developed to determine electrical transport parameters, such as the $\mu\tau$ product. This transport imaging technique has been shown to work well in the 2D case. For the first time, this technique was applied to samples thick enough to undergo 3D diffusion. The 3D case introduces complications to the technique, as the recombination luminescence must be integrated for each layer of the material.

Optical transport measurements were taken on thick GaAs layers to test the technique's accuracy. Diffusion lengths, drift lengths and $\mu\tau$ products were determined in each case. However, the analysis underestimated the values in comparison to published literature. The cause of this error was analyzed and determined to be surface recombination effects. The free surfaces on these samples serve as additional non-radiative recombination sites that affect the luminescence distribution. The results indicate that surface recombination effects must be factored into the analysis. A first estimate of S, the surface recombination velocity, in the 0 V applied bias case has been determined and found to be 6117 cm/s. Developing the ability to extract S and L_{diff} for images taken under applied bias is essential.

In addition to developing and testing transport imaging analysis techniques, the CL of BFO was measured and analyzed. BFO charged intensely in the SEM because it is an insulator. Transport imaging is most effectively performed on less insulating samples because they do not build up such large surface charge effects. Therefore, the optical technique to determine electrical transport parameters would not be effectively used on BFO without some type of doping to improve the conductivity.

The luminescence spectrum of BFO does indicate that there is an optical absorption and potentially emission occurring in BFO between 480 and 576 nm or, equivalently, between 2.15 and 2.58 eV. BFO may still be a potential candidate for the sensing element in a nuclear radiation detector. Due to the bismuth in the compound, BFO has a promisingly high atomic number. Transport imaging in BFO and related oxide materials will require additional research, but may play important roles in the characterization of these new materials.

LIST OF REFERENCES

[1] G. W. Bush, “Remarks by the President to United Nations General Assembly,” U.N. Headquarters, New York, NY, November 2001.

[2] The White House Office of the Press Secretary, “President announces reduction in nuclear arsenal,” in Press conference by President Bush and Russian President Vladimir Putin, November 2001.

[3] S.E. Flynn, “Beyond border control,” *Foreign Affairs*, vol. 79, pp. 57-68, November 2000.

[4] H. Baker and L. Cutler, “A report card on the Department of Energy’s nonproliferation programs with Russia,“ Department of Energy, Washington, D.C., January 2001.

[5] B. D. Milbrath, A. J. Peurrung, M. Bliss, and W. J. Weber, “Radiation detector materials: An overview,” *Journal of Materials Research*, vol. 23, pp. 2561-2581, October 2008.

[6] M. Bunn, A. Wier, and J. P. Holdren, “Controlling nuclear warheads and materials: a report card and action plan,” Harvard University, Boston, MA, March 2003. http://www.guardian.co.uk/world/2009/apr/04/barack-obama-nuclear-weapons

[7] R. S. Quimby, *Photonics and Lasers*. John Wiley and Sons, 2006.

[8] B. V Zeghbroeck, University of Colorado at Boulder, “Principles of semiconductor devices,” 2007, http://ecee.colorado.edu/~bart/book/book/contentc.htm.

[9] W. Freeman, “Imaging transport: optical measurement of diffusion and rift in semiconductor materials and devices,” M.S. thesis, Naval Postgraduate School, Monterey, CA, USA, 2004.

[10] M. L. Boas, *Mathematical Methods in the Physical Sciences.* John Wiley and Sons, 1983.

[11] D. R. Luber, “Direct imaging of minority charge carrier transport in luminescent semiconductors,” M.S. thesis, Naval Postgraduate School, Monterey, CA, USA, 2005.

[12] D. R. Luber, F. M. Bradley, and N. M. Haegel, “Imaging transport for the determination of minority carrier diffusion length,” *Applied Physics Letters*, vol. 88, issue 16, April 2006.

[13] K. S. A. Butcher, D. Alexiev, and T. L. Tansley, “Minority carrier diffusion lengths for high purity liquid phase epitaxial GaAs,” *Australian Journal of Physics*, vol. 46, pp. 317-25, March 1993.

[14] J. S. Blakemore, *Semiconductor Statistics*: Courier Dover Publications, 2002

[15] S. Kawai , T. Masaki, Y. Kato, T. Motooka, “Luminescence from Nd- and Dy-ion-implanted 4H-SiC,” *Applied Physics Letters*, vol. 88, issue 19, May 2006.

[16] S. R. Basu, L. W. Martin, Y. H. Chu, M. Gajek, R. Ramesh, R C. Rai, X. Xu, and J. L. Musfeldt, Photoconductivity in $BiFeO_3$ thin films,” *Applied Physics Letters*, vol 92, issue 9, March 2008.

INITIAL DISTRIBUTION LIST

1. Defense Technical Information Center
   Ft. Belvoir, Virginia

2. Dudley Knox Library
   Naval Postgraduate School
   Monterey, California

3. Professor James H. Luscombe
   Naval Postgraduate School
   Monterey, California

4. Professor Nancy M. Haegel
   Naval Postgraduate School
   Monterey, California

5. Professor Craig F. Smith
   Naval Postgraduate School
   Monterey, California

6. Ensign Sarah L. Catalano
   Naval Postgraduate School
   Monterey, California